

ChronoRAN: Analyzing Latency in 5G Systems

Arman Maghsoudnia
EPFL

Aoyu Gong
EPFL

Raphael Cannatà
EPFL

Dan Mihai Dumitriu
Pavonis LLC

Haitham Hassanieh
EPFL

Abstract– This paper presents ChronoRAN, a mathematical framework for accurately computing one-way latency (for uplink and downlink) in the 5G RAN across diverse system configurations. ChronoRAN models latency sources at every layer of the Radio Access Network (RAN), pinpointing system-level bottlenecks—such as radio interfaces, scheduling policies, and hardware/software constraints—while capturing their intricate dependencies and their stochastic nature. ChronoRAN also includes a configuration optimizer that uses its mathematical models to search through hundreds of billions of configurations and find settings that meet latency-reliability targets under user constraints. We validate ChronoRAN on two open-sourced 5G RAN testbeds (srsRAN and OAI) and a public commercial 5G network, demonstrating that it can closely match empirical latency distributions and significantly outperform prior analytical models and widely used simulators (MATLAB 5G Toolbox, 5G-LENA). It can also find system configurations that meet Ultra-Reliable Low-Latency Communications (URLLC) targets and enable network operators to efficiently identify the best setup for their systems.

1 INTRODUCTION

Introduced in 5G New Radio (NR) to serve mission-critical applications, Ultra-Reliable Low-Latency Communications (URLLC) promises extremely low latency within the Radio Access Network (RAN) stack, aiming for 0.5 ms latency for both uplink (UL) and downlink (DL) channels (1 ms round trip), with high reliability (above 99.999%) [7]. While the specific requirements vary across applications [2], URLLC could revolutionize a wide range of real-time applications [12, 70], including autonomous vehicles [25], industrial automation [13, 18], remote surgery [23], smart grids [29], virtual & augmented reality (VR/AR) [27], professional live audio production [45], and public safety communications [37, 73]. Even conventional applications such as web browsing or gaming can benefit from the improved responsiveness that low-latency 5G networks can provide [61, 69].

Despite the early standardization of URLLC in late 2017 [1], more than a decade of discussions [77], and several years

of commercial 5G rollouts [46], practical 5G deployments cannot consistently achieve the latency and reliability requirements of URLLC [18, 21, 36, 45, 57, 58]. To make matters worse, discussions around 6G indicate even stricter latency goals of 0.1 ms uplink and downlink (0.2 ms round trip) [14, 24, 26, 62]. However, it is still unclear which cellular configurations and system parameters can achieve URLLC in practice. This is because we still lack a clear understanding of latency in the RAN: what are the bottlenecks, how different configuration parameters impact latency, and how they interplay with each other.

Prior work on analyzing latency in the 5G RAN relies on oversimplified models and simulations that do not capture the full system complexity [15, 43, 51, 52, 58, 63, 78]. Widely used simulators, such as MATLAB 5G Toolbox and the ns-3 5G-LENA [50], also fail to reproduce the latency distributions observed in real-world deployments and severely underestimate the latency as we show in §6.

Accurately estimating latency and identifying system configurations that minimize it, however, is challenging. The 5G RAN has hundreds of configuration parameters [22, 39]. Identifying which ones mainly affect latency and correctly modeling their impact is non-trivial. Intricate dependencies among parameters often yield counterintuitive behavior. For instance, prior work has frequently assumed that URLLC can be achieved by simply shortening transmission time slots [20, 33, 66, 74]. In practice, however, using very short slots shifts the bottleneck to processing and radio interface delays. Depending on the chosen TDD (Time Division Duplexing) pattern—which governs the allocation of uplink and downlink slots—packets may miss uplink opportunities or scheduling request windows, ultimately increasing latency rather than reducing it as we show in §6F. Moreover, several variables like processing time, packet arrival time, delays inside the RF radios, etc. are nondeterministic. Analyzing the latency distribution based on the distributions of these random variables quickly becomes intractable.

In this paper, we present ChronoRAN, a mathematical framework that can accurately estimate one-way latency distributions (for both uplink and downlink) inside the 5G RAN stack. ChronoRAN addresses the above challenges through extensive mathematical modeling of the latency sources at

every layer in the RAN stack. We take a system-level approach where we account for various protocol specifications, hardware constraints, and system implementation details and model the dependencies between various configuration parameters. Using these analytical models, ChronoRAN can output the latency for an instantiation of the variables and configuration parameters. To account for nondeterministic components, we collect measurements of non-deterministic variables from an actual 5G system to generate empirical distributions.¹ We then randomly sample these distributions to generate possible instantiations of the distribution.

We also equip ChronoRAN with a configuration optimizer that can find the best configuration for the lowest latency the system can achieve under desired constraints. Through careful pruning, the optimizer can evaluate billions of configurations in a matter of minutes, which would be computationally infeasible using simulators like Matlab and ns-3. ChronoRAN allows us to answer questions like: How can we configure our 5G system to achieve the lowest uplink latency if we restrict our system to operate in the sub-6 GHz bands with a TDD pattern and grant-based scheduling? What are the different configurations that can satisfy 0.5 ms latency with 99.999% reliability? How reliably can we achieve 1 ms latency under a given configuration or traffic pattern?

We implement ChronoRAN and validate its results on two real-world private 5G testbeds with open source RAN implementations, srsRAN [64] and Open Air Interface (OAI) [44], as well as a commercial 5G standalone network. We use synthetic and real application traffic such as video conferencing and gaming to show that the latency distribution calculated by ChronoRAN, accurately matches the real-world latency observed in the testbeds which we quantify using the Wasserstein metric [34, 40, 72]. Our results reveal that:

- ChronoRAN achieves a low Wasserstein distance of 0.003 to 0.035 compared to real-world latency distributions.
- ChronoRAN calculates the lower and upper latency bounds with relative mean errors of 4.8 % and 2.2 %, respectively.
- Compared to prior analytical work [52, 78] and widely used 5G simulators such as MATLAB 5G Toolbox and 5G-LENA [50], ChronoRAN achieves over 40× better Wasserstein distance and over 21× and 35× lower mean absolute error in estimating the min and max latency, respectively.
- Using the ChronoRAN’s configuration optimizer, we find that among feasible configurations in the sub-6 GHz bands, none can meet the URLLC target of 0.5 ms one-way latency at 99.99 % reliability. However, 1.05 % of feasible configurations can satisfy the relaxed target of 1 ms latency at the same reliability level using a Grant-Free configuration.

¹In cases where we lack open source access and cannot directly measure these variables (e.g., user equipment processing time), we learn an approximate distribution from latency measurements.

ChronoRAN is the first mathematical framework to model 5G latency inside the RAN that matches measurements from real 5G networks. ChronoRAN can pinpoint bottlenecks currently preventing URLLC requirements from being met in practice and help configure RAN parameters to minimize latency.

Ethics: This work does not raise any ethical considerations.

2 BACKGROUND

5G NR (New Radio): Similar to 4G LTE, 5G NR uses Orthogonal Frequency-Division Multiplexing (OFDM) at the PHY layer, where the bandwidth is divided into frequency subcarriers on which data is modulated. However, unlike 4G which has a fixed subcarrier spacing (SCS), the SCS in 5G can be selected among seven numerologies (μ). Numerologies 0 to 2 are available in low and mid-frequencies (sub-6 GHz), known as Frequency Range 1 (FR1), while numerologies 2 to 6 are available in the so called mmWaves (24.25 to 52.6 GHz), known as Frequency Range 2 (FR2) [7]. The SCS can be derived as $15 \text{ kHz} \cdot 2^\mu$ [6]. For all numerologies, 14 OFDM symbols are grouped into a time *slot*, with duration $1 \text{ ms}/2^\mu$.

Due to the shared nature of the wireless medium, the base station (gNB) needs to allocate the frequency and time resources to the user equipment (UE). This allocation is known as resource scheduling. After allocation, the gNB sends the results to UEs as part of the DL control information (DCI), which can only be sent once per slot. Consequently, in practice, the scheduling task is done just once per slot. Since the gNB schedules both UL and DL resources, UEs must send a Scheduling Request (SR) via the UL control information (UCI), which the gNB uses to allocate an initial grant.

5G NR supports both FDD and TDD (frequency and time division duplexing). FDD splits the bandwidth into two equal non-overlapping bands that are allocated for the downlink (DL) and uplink (UL) channels [4]. In contrast, TDD uses the entire bandwidth with different time-slots allocated for DL and UL. A TDD period can be composed of one or two consecutive patterns. A pattern consists of several DL slots **D**, followed by one mixed slot **M**, and several UL slots **U**. The mixed slot symbols can be used for DL or UL. TDD offers a more flexible allocation between DL and UL and allows changing the ratio of DL to UL resources on the fly.

5G Network Stack: To understand the 5G stack, we trace the path of a ping request sent by a User Equipment (UE) in a 5G network as shown in Fig. 1, examining the network stacks of both the UE and the gNB. The path begins at the Application (APP) layer in the UE with the creation of a ping request. The data is passed to the PDU (Protocol Data Unit) layer, where a PDU session is established with the core network (UDP/TCP & IP). It then moves through the Service

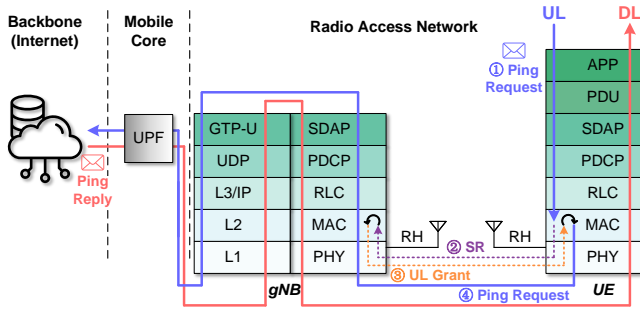


Figure 1: Path of a Ping Request through the 5G Stack.

Data Adaptation Protocol (SDAP) layer for quality of service management and then the Packet Data Convergence Protocol (PDCP) layer for encryption. Next, the data moves through the Radio Link Control (RLC) layer, for segmentation and reassembly. The MAC layer manages access to the shared medium. The UE first sends a Scheduling Request (SR) (② in Fig. 1) and then sends the data after receiving a UL grant (③ in Fig. 1). In the PHY layer, the data is encoded and modulated into samples. The Radio Head (RH) converts these samples into Radio Frequency (RF) signals and sends them to the gNB over the air. On the gNB side, the RH captures the signals and converts them into samples that are then demodulated and decoded into the data. The gNB reconstructs the request from PHY to SDAP and encapsulates it into a General Packet Radio Service Tunneling Protocol User Plane (GTP-U) packet, which is carried toward the UPF through the GTP-U, UDP, IP (L3), L2, and L1 layers. The UPF decapsulates the payload and forwards it to over IP.

The ping reply traces back the same route. However, it can be immediately scheduled for DL transmission at gNB’s MAC layer. The ping journey involves multiple steps contributing to the latency, which we explore in the following section.

3 LATENCY SOURCES

To better understand the nature of latency in 5G systems, we classify each source of delay based on two dimensions: (i) the type of latency source and (ii) its inherent stochastic characteristics (deterministic or non-deterministic). We group latency sources into three main types:

- (1) **Processing latency**: representing the time required for decision-making and data processing.
- (2) **Protocol latency**: introduced by protocol mechanisms and configurations.
- (3) **Radio latency**: covering the time spent in the radio front-end (RH) and its interactions with the physical layer.

For simplicity, we start with a high-level analysis, which we formalize in the following section. We detail the ping journey in Fig. 1 from a temporal perspective and present a breakdown in Fig. 2. While larger packets and buffer waiting times add complexity—requiring additional buffer reports

and grants—the underlying high-level principles remain consistent across scenarios. Consequently, we defer the formal analysis and modeling of these more complex cases to the appendix, though we keep their evaluation to demonstrate the generalizability of our analysis and model.

For a ping request, the UL transmission begins at the UE in ①. The UE prepares the scheduling request (SR), processing through the layers from APP down to PHY (APP↓), to request network resources. However, the UE must wait for the next UL slot to respect the TDD pattern. ② The UE transmits the SR in the next UL slot to the RH at the gNB side. ③ The RH passes samples to the PHY layer, where they are demodulated and decoded. The MAC layer receives the SR and schedules a UL grant for the UE. The scheduling (SCHE) does not occur right away, as it is performed periodically in every slot. ④ Consequently, the grant is scheduled in the next slot. ⑤ Afterward, the gNB sends the grant to the UE as part of the control information. ⑥ After the UE receives the grant, it waits for the next UL slot and sends the ping request to the gNB (↑MAC↓). ⑦ Finally, the gNB processes the UL data samples and passes the ping request to the UPF through the layers from MAC up to SDAP (MAC↑).

For the ping reply, the DL transmission begins at the gNB in ⑧. The gNB processes the DL data through the layers from SDAP down to RLC (SDAP↓). ⑨ Again, as the scheduling is performed periodically in every slot, the data waits in the RLC layer and is scheduled in the next slot. ⑩ Next, the scheduling result specifies the DL slot where the data will be transmitted to the UE. ⑪ Finally, the UE receives the DL data in one or multiple symbols of the DL slot. It then passes the data through the layers from PHY up to APP (PHY↑).

Given the breakdown, the three latency sources are summarized as follows. (i) The *processing latency* exists in both UE and gNB (cf. ①, ④, ⑥–⑨, ⑪). This latency includes the time taken for processing data through the layers from APP down to PHY in the UE and from PHY up to SDAP in the gNB. (ii) The *radio latency* (\mathbb{R}) also appears in both the UE (cf. ②, ⑤, ⑥, ⑪) and gNB (cf. ③, ⑦, ⑩). This latency consists of the time spent in RF chains (e.g., analog-to-digital and digital-to-analog conversions), queuing delays on interface buses, and the bus transmission time. (iii) The *protocol latency* is the most significant, including the configurations in use (cf. ①, ④, ⑥, ⑦, ⑨). Specifically, the SR and grant procedure noticeably increases the latency of UL transmissions (cf. ②–⑤). An alternative grant-free access mechanism allocates resources to UEs without SRs, reducing latency but facing scalability issues as the number of UEs increases [9].

It is crucial to note the following points:

- These latency sources can be influenced by numerous factors specific to the system in use. For instance, in software-based 5G implementations, processing latency may increase or be

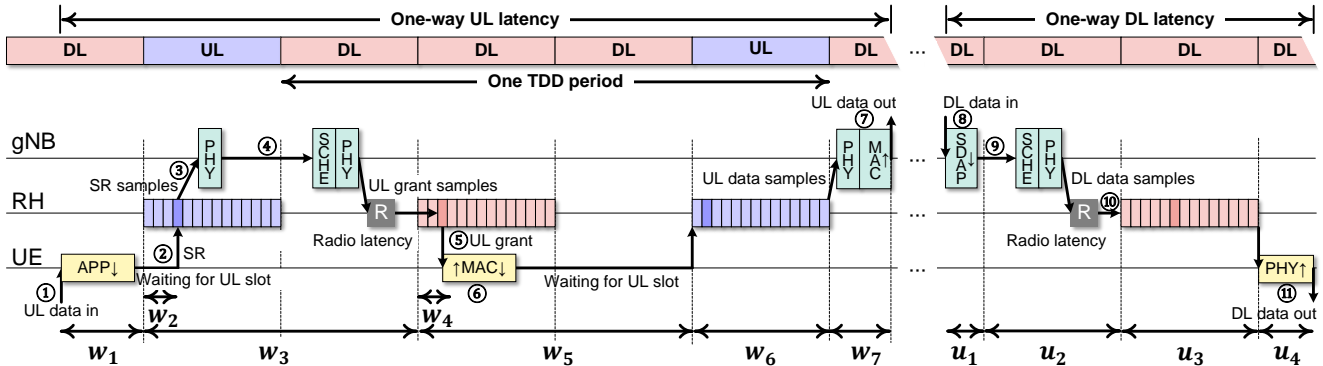


Figure 2: Overview of the system-level latency along the path of a packet with *TDD Common Configuration of DDDU* pattern.

random due to the non-real-time nature of operating system (OS) scheduling. Radio latency also varies with the type of interface—PCIe, QSFP, Ethernet, or USB—used to connect the radio head (RH) to the processor running the 5G stack.

- *These sources are also interdependent.* For instance, the MAC scheduler must be designed to account for the total processing time in subsequent layers and radio latency. Failure to do so may result in the radio not being ready for transmission, leading to a corrupted signal. Since the sum of these delays is non-deterministic, practical implementations require the scheduler to include a margin to ensure the radio is ready on time, further increasing latency.

- *Any of these sources can bottleneck the system.* For instance, if the radio latency is 0.5 ms, selecting a shorter TDD pattern may not reduce latency and could even increase it. In particular, if the latency exceeds one TDD pattern in the *DU* configuration, an entire pattern is missed before the gNB can respond to the scheduling request. Although counter-intuitive, it is preferable to increase the TDD pattern duration to *DDUU*, allowing responses to scheduling requests without missing a full pattern as we show in detail in §6F.

4 CHRONORAN

4.1 Formal Models

In this section, we present our mathematical modeling of latency in 5G systems. **We focus on latency inside the 5G RAN. We model the DL latency as the time for a packet to travel from the beginning of the SDAP layer at the gNB, shown in Fig. 1, to the end of the SDAP layer at the UE, and the UL latency as the time for a packet to travel in the reverse direction.** Due to the complexity of modeling the system, we split our analysis into several cases. While some cases can be merged, it is easier to follow the analysis by slowly building up the model to make it more general and then addressing some special cases:

- (1) UL latency for size 1 packets in TDD
- (2) UL latency for size 2 packets in TDD
- (3) UL latency when radio delay > TDD period

- (4) UL latency for packet trains in TDD (RLC layer buffering)
- (5) UL latency with grant-free access
- (6) DL latency in TDD
- (7) UL and DL latency with Mini-Slot configuration
- (8) UL and DL latency in FDD
- (9) UL latency under multi-UE contention

We start by analyzing the uplink latency in TDD, similar to the ping request example shown in the previous section. We define two sizes of packets:

- **Size 1:** Packets that can be fully transmitted in the initial resources granted by the gNB to the UE following the SR (scheduling request).

- **Size 2:** Larger packets that require additional resources. We further extend the model to account for a train of back-to-back packets where buffering at the RLC layer is modeled, the case when the radio latency is large, and grant-free access, which is a configuration that allows uplink transmissions to skip the scheduling request and immediately transmit in preallocated resources. We also analyze downlink latency as well as the mini-slot configuration² and FDD. Finally, we analyze uplink latency with multi-UE contention. Due to limited space and the increased complexity of the mathematical models, we will present the formal model for the first case and defer the remaining cases to the Appendix E. However, the analysis follows similar logic, and we will provide an evaluation of all these cases in §6.

Modeling of the Uplink Latency Case 1: We break the total latency into distinct components, as illustrated in Fig. 2 for uplink transmissions. The total UL latency is the sum of the consecutive components (Fig. 2) expressed as follows:

$$\text{Total UL Latency} = w_1 + w_3 + w_5 + w_6 + w_7 \quad (1)$$

In the following, we describe each component in detail.

Modeling w_1 : This variable represents the time from packet generation until the scheduling request is transmitted for that packet. It includes both the UE’s preparation time for the scheduling request message and the wait time for the

²A special case where a time-slot can have both DL and UL symbols.

next available uplink slot. Two configurable parameters, the *Scheduling Request Periodicity* (SR_P) and the *Scheduling Request Offset* (SR_O), determine when scheduling requests can be sent. The offset indicates the first slot (relative to the gNB's start) in which a scheduling request can be transmitted, and the periodicity specifies the interval (number of time slots) between consecutive scheduling requests. Let T be the number of time slots in the TDD pattern. Then, the scheduling request (SR) can only be sent in time slots: $\{SR_O + \{1, \dots, T\} \cdot SR_P\}$. However, some of these slots might be DL, and the SR must be sent in a UL slot.

To find w_1 , we must identify all possible UL slots for scheduling requests. The earliest slot after the UE is ready determines w_1 . Let d be the number of downlink slots in the TDD pattern. Hence, the UL slots in the TDD pattern are $\{d + 1, \dots, T - 1\}$. The problem can be written as:

Find the largest set $A = \{k'_0, k'_1, \dots, k'_{T'-1}\}$, such that:

$$A \subseteq \{1, \dots, T\}, \quad k'_0 < k'_1 < \dots < k'_{T'-1}, \quad (2)$$

$$SR_O + A \cdot SR_P \equiv_T B \quad (3)$$

$$B \subseteq \{d + 1, \dots, T - 1\}, \quad (4)$$

where $\{SR_O + A \cdot SR_P\}$ is the set of uplink slots in which we can send an SR, and \equiv_T is the set equal operator modulo T . Eq. (2) limits the solution to a finite set, Eq. (3) ensures that scheduling requests are sent in slots dictated by the offset and periodicity, and Eq. (4) ensures that scheduling requests are sent in uplink slots.

LEMMA 4.1. *Let $n = \text{GCD}(SR_P, T)$, $\varphi(\cdot)$ be Euler's totient function, and define the set $D = \left\{ \left\lceil \frac{d+1-SR_O}{n} \right\rceil, \dots, \left\lfloor \frac{T-1-SR_O}{n} \right\rfloor \right\}^3$, then:*

$$A = \left\{ \left(j \cdot \left(\frac{SR_P}{n} \right)^{\varphi\left(\frac{T}{n}\right)-1} \bmod \frac{T}{n} \right) + \frac{T}{n} i \mid j \in D, i \in \{0, \dots, n-1\} \right\}$$

The proof of this lemma can be found in Appendix A.

Now that we have found A , we know the slot numbers where the scheduling request can be sent. We define o_1 as the time the packet is generated relative to the gNB's start (zero time reference). Assuming the UE needs l_1 seconds to prepare the request after data generation, and each slot is S seconds, we can calculate the first slot in which the UE is ready to send the request after SR_O as:

$$SR_{\text{ready}} = \left\lceil \frac{o_1 + l_1}{S} \right\rceil - SR_O \quad (5)$$

Since the SR slots are periodic of period $T \cdot SR_P$ (with respect to the location they occupy in the TDD pattern), define quotient of the division of SR_{ready} by $T \cdot SR_P$ as q and the remainder as r .

$$q = \left\lfloor \frac{SR_{\text{ready}}}{T \cdot SR_P} \right\rfloor, \quad r = SR_{\text{ready}} \bmod T \cdot SR_P \quad (6)$$

³ $D = \emptyset$ if $\left\lceil \frac{d+1-SR_O}{n} \right\rceil \geq \left\lfloor \frac{T-1-SR_O}{n} \right\rfloor$

w_1 is calculated based on a simple intuition as follows. We locate the slot where the UE is ready to send the scheduling request. Then we identify the next slot in which the scheduling request can be sent.

$$w_1 = \begin{cases} S(SR_O + (k'_0 + qT)SR_P) - o_1 & \text{if } r < k'_0 \cdot SR_P \\ S(SR_O + (T + k'_0 + qT)SR_P) - o_1 & \text{if } r > k'_{T'-1} \cdot SR_P \\ S(SR_O + (k'_{i+1} + qT)SR_P) - o_1 & \text{if } k'_i < \frac{r}{SR_P} < k'_{i+1} \end{cases} \quad (7)$$

$$i \in \{0, \dots, T' - 2\}$$

Modeling of w_2 : This variable represents the time at which the scheduling request is sent relative to the slot's start. The request is transmitted via the Physical Uplink Control Channel (PUCCH) within that slot. Each 5G slot has 14 symbols, and the scheduling request is sent in one of these symbols. The standard allows one or more contiguous symbols for PUCCH. We call the first symbol UC_{st} and the number of symbols UC_{no} . Consequently, w_2 can be calculated as:

$$w_2 = \frac{UC_{st} + UC_{no}}{14} \cdot S, \quad UC_{st} + UC_{no} \leq 14 \quad (8)$$

Modeling of w_3 : This variable represents the time between the beginning of the slot that sends the scheduling request and the DL slot delivering the UL grant. The gNB processes the scheduling request and issues a grant to the UE, specifying resources and time slot for data transmission. Like UL control information, the grant is sent via the Physical Downlink Control Channel (PDCCH) in the slot where it appears. Let:

- p_1 : The gNB's processing time for the scheduling request.
- p_2 : The MAC layer's processing time for allocating resources based on the UE's demands.
- p_3 : The physical layer's processing time for generating radio samples for transmission.

Typically, the MAC layer processes the grant at the start of each slot, followed by the physical layer. Therefore, we can express the time at which the MAC starts processing the grant as follows:

$$\text{Start of MAC Processing} = o_1 + w_1 + \left\lceil \frac{w_2 + p_1}{S} \right\rceil \cdot S \quad (9)$$

The physical layer must timestamp the samples before submitting them to the radio for transmission. The radio processes these samples and transmits them at the designated time. If the gNB does not provide enough lead time, the radio may fail to process and transmit the samples in time, resulting in underflow and data loss. Hence, the gNB must supply the samples to the radio in advance. We define the number of slots the MAC schedules in advance as a_1 . The time the radio needs to prepare the samples before transmission is r_1 . Based on this, two constraints apply. First, MAC and physical layer processing must finish before radio processing begins. Second, the radio must have enough time to prepare the samples before transmission, expressed respectively as follows.

$$\left\lceil \frac{p_2 + p_3}{S} \right\rceil \leq a_1 + 1, \quad r_1 < (a_1 + 1) \cdot S - (p_2 + p_3) \quad (10)$$

The scheduled slot for grant transmission is as follows:

$$\text{Scheduled Slot for Grant} = \frac{o_1 + w_1}{S} + \left\lceil \frac{w_2 + p_1}{S} \right\rceil + a_1 + 1 \quad (11)$$

The value of w_3 can be calculated as follows. The cases follow the logic that the scheduled slot for the grant should be a DL slot. If the slot determined by Eq. (11) is a UL slot, the grant is sent in the first DL slot of the next TDD period (second case in Eq. (13)).

$$re_1 \equiv_T \frac{o_1 + w_1}{S} + \left\lceil \frac{w_2 + p_1}{S} \right\rceil + a_1 + 1 \quad (12)$$

$$w_3 = \begin{cases} \left(\left\lceil \frac{w_2 + p_1}{S} \right\rceil + a_1 + 1 \right) \cdot S; & \text{if } re_1 \leq d \\ \left(\left\lceil \frac{w_2 + p_1}{S} \right\rceil + a_1 + 1 + (T - re_1) \right) \cdot S; & \text{otherwise.} \end{cases} \quad (13)$$

Modeling of w_4 : This variable represents the time at which the grant is sent relative to the beginning of its slot. The grant is carried in the PDCCH within the slot. Only the slot's start can be used for the PDCCH, and the standard limits PDCCH to at most three symbols. Let DC_{no} be the number of symbols used. Consequently, w_4 can be calculated as follows:

$$w_4 = \frac{DC_{no}}{14} \cdot S, \quad DC_{no} \in \{1, 2, 3\} \quad (14)$$

Modeling of w_5 : This variable represents the time between the beginning of the slot in which the grant is sent and the UL slot where the UE sends data using the allocated resources. Each grant in PDCCH includes information specifying the slot in which the UE should send data. This slot is communicated using an offset value called k_2 , which indicates how many slots after the grant the UE should transmit. The value of k_2 must align with the UE's processing capability. If the UE requires l_2 seconds for MAC and PHY processing, the minimum value of k_2 can be calculated as follows. This equation determines the first slot after the grant where the UE is finished with the processing.

$$k_{2_{\min}} = \left\lceil \frac{w_4 + l_2}{S} \right\rceil, \quad k_{2_{\min}} \leq k_2 \quad (15)$$

If we assume that the grant aims to minimize latency by setting k_2 as low as possible, w_5 can be calculated as:

$$re_2 \equiv_T \frac{o_1 + w_1 + w_3}{S} + k_{2_{\min}} \quad (16)$$

$$k_2 = \begin{cases} k_{2_{\min}}, & \text{if } re_2 \geq d; \\ k_{2_{\min}} + d - re_2, & \text{otherwise.} \end{cases}, \quad w_5 = k_2 \cdot S \quad (17)$$

Eq. (16) calculates the slot number within a TDD period. The second case in Eq. (17) represents the scenario where the $k_{2_{\min}}$ -th slot after the grant is a DL slot. In this case, the grant must be postponed until the next available UL slot, which is the first UL slot in the same TDD period.

Modeling of w_6 and w_7 : w_6 represents the time of the UL data transmission. If we assume that the UL data can be transmitted within a single Physical Uplink Shared Channel (PUSCH) slot (more complex cases are addressed in the appendices), $w_6 = S$. Once the uplink data reaches the gNB

radio, it must be forwarded and processed through all layers of the 5G stack before being forwarded to the core network. This processing time is represented by w_7 . We aggregate the processing time across all 5G stack layers into a single variable, p_4 . Hence, $w_7 = p_4$. While gNB processing could be improved to occur symbol by symbol (as with PDCCH and PUCCH), we assume it begins only after the entire slot is received (Fig. 2). This worst-case assumption accounts for uncertainty in the symbol carrying the data and the likelihood that large transmissions span most of the slot.

4.2 Stochastic Framework

In § 4.1, we introduced a model for system latency using several variables. However, some of these variables are non-deterministic and fluctuate over time. For example, the values of the *UE Processing Time* (denoted by l_1) and the *gNB Processing Time* (denoted by p_4) can substantially affect overall latency. To appreciate the need to model the stochastic nature of these variables, consider a 5G system where the scheduling request (SR) period is set to 20ms. If a UE is idle and suddenly has a new packet to send, it must wait for the next SR opportunity before transmission. Suppose the next SR window is 1ms away, and the UE's processing time averages 1ms but has some variability. In this case, the UE may miss the imminent SR window due to longer-than-average processing, incurring an extra 20ms delay until the following SR opportunity. Similarly, the gNB processing time varies depending on the system load, contributing to non-deterministic latency.

Because of these uncertainties, latency must be examined from a probabilistic perspective. In particular, there are two types of variables defined in § 4.1: (1) Constants dictated by the chosen system configuration, such as S , the time slot duration, and T , the number of time slots in a TDD pattern. (2) Random variables like o_1 (the data packet arrival time), l_1 and p_4 mentioned above. To generate the output distribution for the latency, we sample these variables from their input distribution. For each sampling instance of the random variables, we calculate the latency. We then aggregate the latency measurements across samples to generate the latency distribution. The input distribution of these random variables can be either:

(A) *Empirical distribution:* The empirical distribution is generated by collecting real measurements of the values of these random variables from an experimental setup and aggregating them to generate a probability density function (PDF).

(B) *Learned distribution:* In some cases, it is not feasible to directly measure these variables since the 5G UE chipsets are not opened (e.g. Qualcomm SDX65 [56]). To address this, we learn the distribution by assuming it follows a known distribution (e.g., Gaussian with mean μ and standard deviation σ). We then collect the latency of 10 000 packets sent with

constant inter-arrival time as our ground truth on a given configuration and find the final output distribution of the latency. We iterate over different parameters (e.g., μ and σ) of the input distribution and generate the output latency distribution using the models as described above. We then use the Wasserstein distance [34, 40, 72] as our error function between the calculated and measurement distributions to find the best parameters that fit the real-world data. By doing so, we can indirectly estimate the input distribution of these random variables. It is important to note that we only learn the distribution (train) from a single configuration. However, we evaluate it (test) on completely new configurations that generate very different output latency distributions.

In this paper, we focus on the three important variables:

UE Processing Time (l_1 in §4.1). We learn the distribution of this variable by assuming it is a Gaussian, which seems to match well. Note, however, that depending on the UE’s load, the processing time can vary in the range of 2 ms. The typical UE’s processing time mean in our experiments is around 1 to 3 ms, and the standard deviation is around 0.1 to 0.6 ms for low and high loads, respectively. Since the variation in processing time is insignificant with respect to the load, we train the parameters on a certain load and use it to test the model with different configurations and loads.

gNB Processing Time (p_4 in §4.1). Modeling the gNB processing time can be easier than the UE processing time, due to our access to the open-source gNBs. However, for closed gNBs, we can also use a learned distribution since we find that the empirical distributions can be approximated with a log-normal distribution. Typically, the mean processing time of the gNB in our experiments is around 0.5 – 1.66 ms for low and high loads, respectively; the standard deviation is around 0.1, and the location parameter is around 0.3.

Packet Inter-Arrival Time (related to o_1 in §4.1). The random variable o_1 is for packet generation time. The distribution of such a variable is not very meaningful. Instead, to generate values of o_1 , what we really need is the distribution of packet inter-arrival times. We can easily measure o_1 from logs at the gNB or UE and use it to generate a distribution of packet inter-arrival times. We then sample this distribution and use the inter-arrival times to generate new values of o_1 , which we then use to output the latency distribution.

4.3 Configuration Optimizer

Finding the right configuration for a 5G gNB is far from a trivial task. This involves tuning many parameters. Some parameters might be fixed by the standards, like the use of TDD pattern (to synchronize with neighboring cells) or the use of FDD in the sub 2.6 GHz bands [4], while others have to be set by the operators. A naive approach, like setting all

the free parameters to the minimal value, might result in a worse latency, as we show in §6F.

We design an optimizer that systematically explores the configuration space to identify the best valid configuration for a gNB under a given set of constraints. The objective for the best valid configuration can be user-defined, such as minimizing the average latency or the 99% latency of the distribution. Despite the fact that we restrict the search to parameters that mainly affect latency, the configuration space still grows combinatorially, with around 32 billion in the sub-6 GHz frequency bands grant-based access alone. This number arises from the range of possible values of each configuration parameter as detailed in §C.

To make the search tractable, we reduce the configuration space through systematic pruning based on three principles. First, each parameter value is validated against 5G standard constraints, ensuring that only standard-compliant configurations are considered. For example, the slot duration is restricted to $2^u \times 1$ ms, where $u \in \{0, 1, 2\}$ in the sub-6 GHz bands and $u \in \{2, 3, 4, 5, 6\}$ in the millimeter-wave bands. This step eliminates many invalid configurations. Second, the optimizer accounts for cross-parameter dependencies that can make otherwise valid individual settings infeasible when combined. For instance, if the scheduling request (SR) period and SR offset are chosen independently of the TDD pattern, the SR may always fall in a downlink slot, preventing the UE from transmitting an SR. Similarly, the number of slots in a TDD pattern and the slot duration cannot be set independently, since their product (the TDD period) is restricted to specific values by the standard. Finally, for parameters whose impact on latency is monotonic, the optimizer fixes them to their optimal values to further reduce the search space. For example, placing UL control information at the beginning of a slot ensures that scheduling requests are sent and received earlier, and varying this parameter cannot improve latency. After pruning, the remaining valid configurations are evaluated in two phases. In the coarse phase, the optimizer runs the ChronoRAN model using a few packets to estimate latency distributions and retains the top 10 % of configurations. In the finer phase, it evaluates these candidates with a larger number of packets to identify the best configuration according to the chosen objective (e.g., mean or minimum latency).

In addition to identifying the single best configuration under a chosen objective, the optimizer also supports find-all-configurations that satisfy a given objective. In this case, the optimizer disables optimizations such as fixing parameters with monotonically decreasing latency effects and the two-phase coarse-fine search, since these mechanisms are designed to eliminate non-optimal configurations rather than output all valid ones. It allows us to answer questions like:

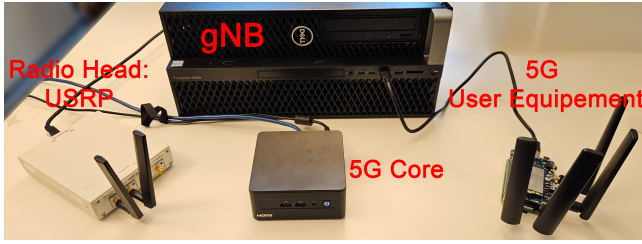


Figure 3: The private 5G testbed setup.

- What configurations can achieve a 1 ms uplink latency with a reliability of 95 % given that we use numerology 3?
- Is it possible to achieve 0.5ms downlink latency with a reliability of 99.99 % if the radio latency is 0.3 ms?
- What configurations can achieve URLLC specs without using Grant Free Scheduling?
- What configuration achieves the lowest average latency given the constraint that we must use TDD with a period of 6 slots (4 DL and 2 UL)?

For reliability, we follow the definition provided in the 3GPP standard [7] which defines reliability as the probability that packets of a given size are successfully delivered within a specified latency bound. In particular, [7] specifies that for URLLC, the target reliability is $1 - 10^{-5}$ for packets of 32 Bytes delivered within 1 ms. ChronoRAN assumes no packet loss. Therefore, the reliability we report reflects whether a given configuration, together with the stochastic components of the system, can meet the latency–reliability target defined by the standard under ideal channel conditions. We believe this perspective is more informative for assessing latency feasibility than focusing solely on packet loss. Consequently, since packet losses may occur in practice, the reported reliability is not guaranteed to hold in real deployments, but it serves as an indicator of whether the system can satisfy the target reliability when channel conditions are favorable. Accordingly, reliability can be inferred from the CDF of the output latency distribution. For example, if the maximum of the 99 % percentile latency is 3 ms, then the system achieves 3 ms latency with 99 % reliability.

5 IMPLEMENTATION AND SETUP

Private 5G Testbed: We evaluate ChronoRAN on two private 5G networks deployed in our lab. We use modified versions of commonly used open-source 5G RAN implementations, namely srsRAN [64] and OpenAirInterface (OAI) [44], and an open-source core network implementation, Open5GS [47]. For our radio platform, we use the USRP B210 and BladeRF xA9. We run the gNB code on an Intel Xeon W-2225 CPU. Furthermore, we use Telit FN990A40 5G modems as UEs. The testbed is shown in Fig. 3. Due to the constraints of the open-source 5G implementations, for TDD, we obtain ground truth latency measurements using band n78 with a SCS of 30 kHz, and for FDD, we obtain measurement using

band n3 with a SCS of 15 kHz. We evaluate different FDD and TDD configurations, such as 2 ms, 2.5 ms, and 5 ms TDD periods, with different TDD patterns and different SR periods. Moreover, we evaluate both grant-based and grant-free access modes.

Commercial 5G Network: We also evaluate ChronoRAN using latency measurements collected from a public commercial mobile network operator (MNO). MNO is the only operator in our country that provides 5G Standalone (SA) service to consumers at this time. Measurements were conducted using a Quectel RM500Q-GL 5G modem with a consumer-grade 5G data plan. To measure one way latency, packets were transmitted from the UE to our synchronized server over the public Internet as we do not have access to MNO’s RAN. Packets therefore traverse the 5G RAN, the mobile core network, and the public Internet. For uplink measurements, sending both ICMP or UDP packets from the UE to the server is feasible. For downlink measurements, due to NAT and firewall restrictions, the server cannot directly initiate connection to the UE; therefore the UE first sends ICMP packets to the server, which then replies to the UE.

The measured end-to-end latency includes additional wired-network delays from the core and the Internet, which cannot be isolated from the 5G RAN in commercial deployments. Moreover, ChronoRAN requires network configuration parameters to compute latency distributions. We obtain these parameters by decoding RRC messages captured with QC-Super [60], which interfaces with Qualcomm-based devices to record raw 5G radio frames. This allows us to extract key settings such as the numerology, TDD pattern, and SR period. However, some parameters (e.g., a_1) remain unobservable. Through extensive measurements, we find that the wired delays appear as an additive Gaussian component on top of the RAN latency. Therefore, we perform a parameter sweep over the unknown model parameters (e.g., a_1 and the Gaussian mean and variance) using one measurement trace, selecting the best match to the observed latency distribution. The learned parameters are then reused for new measurements in §6. Parameters of MNO, either learned or directly obtained by decoding RRC messages, are summarized in §D.

ChronoRAN: To evaluate ChronoRAN, we implemented all the models summarized in §4.1 in Python. The implementation can operate in two modes: (1) Synthetic-traffic: generated with specific traffic-arrival distribution and packet sizes, and (2) Real-traffic: replayed from previously captured application traffic. We use a custom-built C-based traffic generator and replayer to achieve precise inter-arrival times for both synthetic and replayed traffic, outperforming conventional baseline generators [8, 41, 59], as shown in Appendix B.2. We also implemented a separate module for the configuration

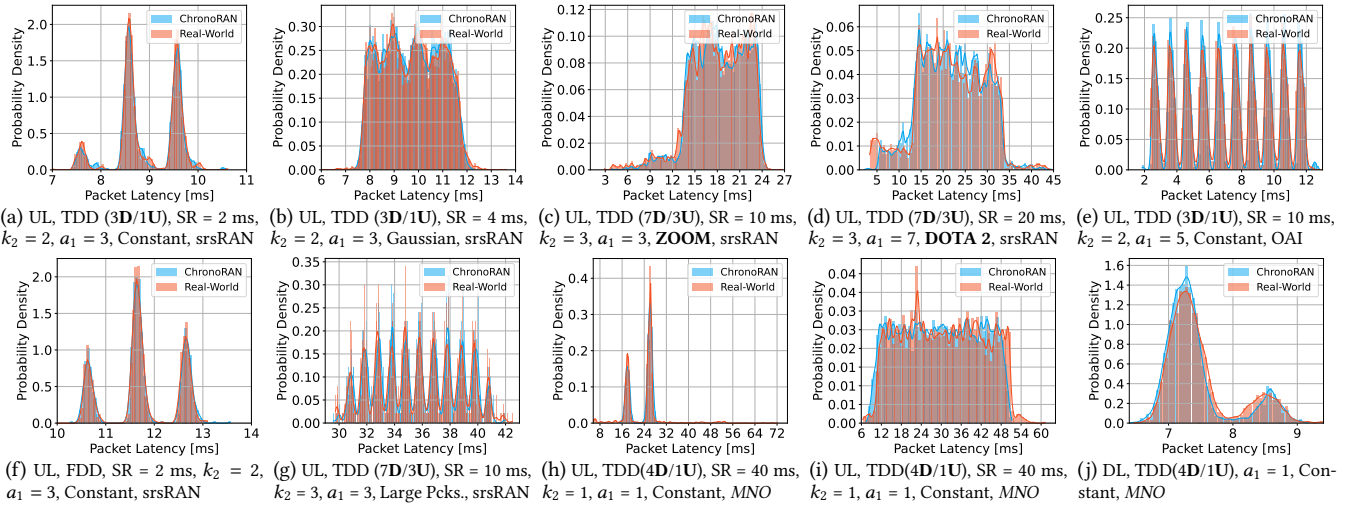


Figure 4: Latency distribution up to the 99th percentile across scenarios on a commercial 5G operator (*MNO*) and two private 5G testbeds (*srsRAN*, *OAI*). Traffic includes real applications (Zoom, DOTA 2) and synthetic workloads: (1) Constant—64 bytes packets with fixed inter-arrival time (101–1000.01 ms); (2) Gaussian—64 bytes packets with Gaussian inter-arrival times (mean 105 ms, std 0.05 ms); (3) Large packets—40 000 bytes packets with fixed 201 ms inter-arrival time. Panels (a–e,g–j) use numerology 1; panel (f) uses numerology 0.

optimizer. Since each configuration can be evaluated independently, the optimizer lends itself naturally to parallel and distributed execution. We employ the Ray framework [30] to run the code across 14 machines simultaneously to obtain the results in §6G.

6 EVALUATION

A. ChronoRAN Accuracy: We first demonstrate how our model can accurately determine latency distributions and bounds (max and min). In Fig. 4, we show the comparison between the latency distribution estimated by ChronoRAN and the latency distribution measured in a public commercial 5G operator (*MNO*) and our real-world 5G testbed based on *srsRAN* or *OAI* under various system conditions (all denoted by *Real-World*). Using our 5G testbed, we have the flexibility to evaluate the model across different frame structures, SR periods, offsets k_2 , MAC’s in-advance scheduling slots a_1 , packet arrival patterns, implementations (*srsRAN* and *OAI*), UL and DL channels, duplexing (FDD and TDD configurations), and varying packet sizes. For the commercial 5G network, we run experiments in an urban outdoor non-line-of-sight environment during peak hours, approximately 5pm–9pm [76], with the device located approximately 1 km from the serving cell tower.⁴ We evaluate ChronoRAN under both our own generated traffic (e.g., with constant and Gaussian inter-arrival times) and traffic from operational

⁴We have noticed that during peak hours, *MNO* uses dynamic SR periods that likely adapt to network conditions (e.g., load). Since we have access to the RRC messages, we constantly extract the SR period and update the corresponding value in ChronoRAN for each packet transmission.

applications (Zoom video calls and DOTA 2 online gaming data).⁵ We can observe from all the cases in Fig. 4 that our model can closely match the real-world latency distributions, accurately capturing the distribution range and the overall shape. This consistency demonstrates our model’s capability of replicating both the spread and the structural characteristics of the measured latency distributions. We present ten additional scenarios in §B.1. We also verify ChronoRAN’s capability to determine latency lower and upper bounds. Fig. 5 shows that ChronoRAN is able to accurately match these bounds across various 5G configurations.

Finally, we use the *Wasserstein distance* [34, 40, 72] to quantify the difference between the estimated and measured latency distribution, and we present the results in Fig. 6. This metric represents the minimum “cost” of turning one distribution into another. We can see from Fig. 6 that the average values on the normalized distributions range from 0.003 to 0.035 which is considered very accurate in practice [48].

B. Multi-UE Scenario: ChronoRAN also models latency under multi-UE contention (see §E.8). Since contention dynamics depend on the scheduling policy at the gNB, we model the round-robin scheduler used in our testbed. The same framework can be readily extended to incorporate other scheduling strategies. Fig. 7 presents latency distributions when four UEs connect to a single gNB and contend for

⁵Note that for such applications, most traffic arrives in bursts/trains rather than as a steady stream. Therefore, accurately capturing this bursty behavior requires modeling buffering effects at the RLC layer. Due to space limitations, the corresponding model is presented in §E.3 and Fig. 19, while its evaluation is included in Fig. 4c–d.

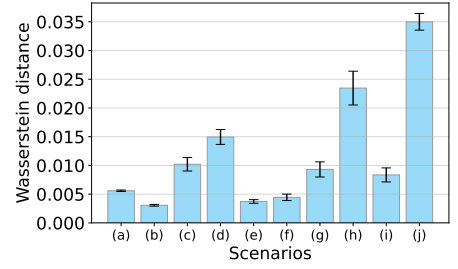
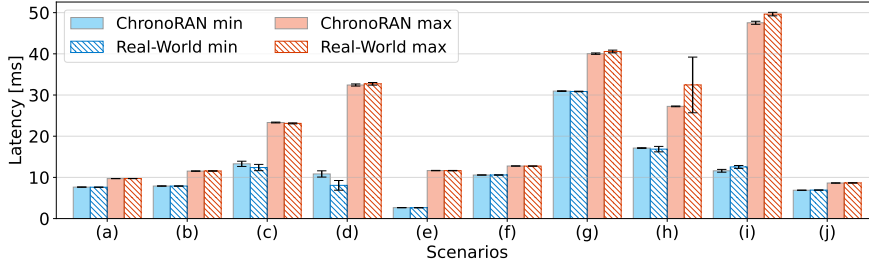


Figure 5: Latency bounds within the 5th-95th percentile range comparing ChronoRAN and Real-World under the same scenarios as Fig. 4.

Figure 6: Wasserstein distances between ChronoRAN and Real-World.

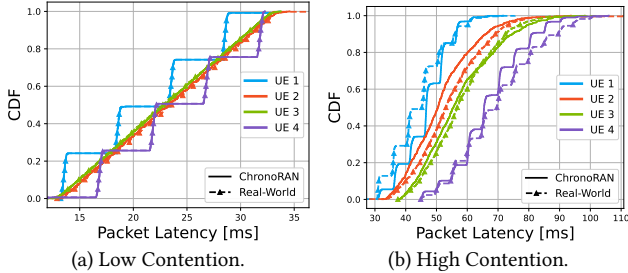


Figure 7: Latency distribution with contention from 4 UEs.

uplink access. We evaluate two operating regimes: low contention, where each UE generates traffic at an average rate of 70 kbps (Fig. 7a), and high contention, where the average per-UE rate is 5.6 Mbps (Fig. 7b). In the high contention case, the total offered load (22.4 Mbps) saturates the full capacity of our 20 MHz testbed. Under low contention, representative of many URLLC scenarios [35], ChronoRAN closely matches the measured latency distributions. Even under high contention, it continues to track the overall distribution trends, with minor deviations as contention effects become more pronounced. Besides these testbed experiments, the commercial-network results for *MNO* in Fig. 4 also inherently include contention effects, since the RAN is shared with other commercial users whom we cannot be aware of. Nevertheless, ChronoRAN continues to accurately capture the latency.

C. Comparison to Prior Work: In §6, we compare ChronoRAN against two baselines—Patriciello19 [52] and Zhao23 [78]—under the following configuration: uplink, TDD (3D/1U), SR = 2 ms, $k_2 = 5$, $a_1 = 7$, Constant, srsRAN. Patriciello19 assumed a fixed two slots gNB processing time and focused solely on the FDD configuration, while Zhao23 examined different duplexing but neglected hardware processing time. For a fair comparison, we modify Patriciello to support TDD configurations and enable both models to process recorded traffic. Both baselines significantly underestimate latency, resulting in distributions that deviate considerably from the real-world distribution, with average Wasserstein distances of 0.63 and 0.83. The errors primarily arise from: 1) The baselines failed to identify system bottlenecks, leading to an underestimation of the required TDD periods for finishing UL

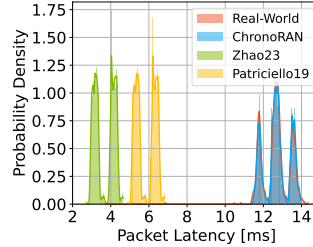


Figure 8: Distributions of ChronoRAN and baselines.

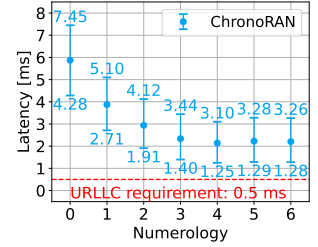
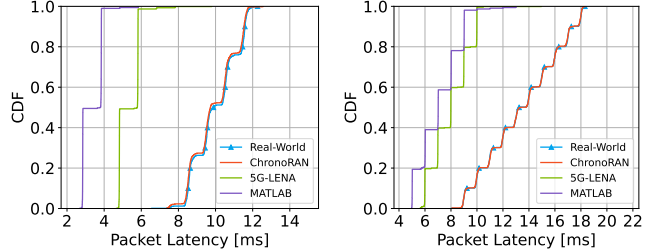


Figure 9: UL latency values (min, avg, and max) vs μ .



(a) Uplink, TDD (3D/1U), SR = 4 ms, (b) Uplink, TDD (7D/3U), SR = 10 ms, $k_2 = 2$, $a_1 = 3$, Constant, srsRAN $k_2 = 3$, $a_1 = 3$, Constant, srsRAN

Figure 10: Comparison of latency distributions between ChronoRAN and two 5G simulators for two scenarios.

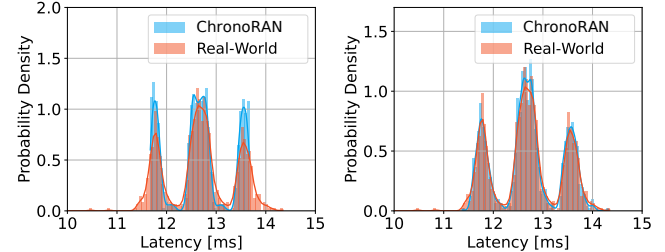


Figure 11: Comparison of modelling l_1 and p_4 as random variables (right) versus constant values (left)

transmissions. 2) They did not account for non-deterministic components, resulting in substantial distortions in the distribution. In contrast, our model matches the measured results with a Wasserstein distance of 0.01.

D. Comparison with 5G Simulators: One might ask: *Why develop a new analytical model for latency estimation instead of relying on existing 5G simulators?* To address this, we evaluated ChronoRAN against two 5G simulators: the MATLAB 5G Toolbox [31], and 5G-LENA [50], an open-source

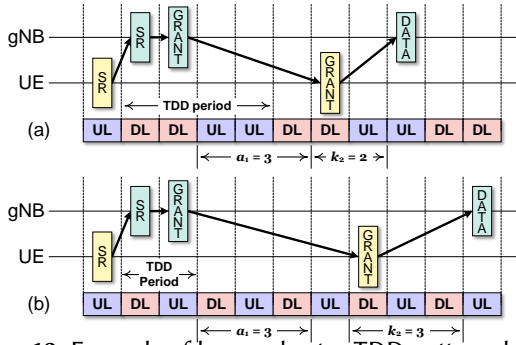


Figure 12: Example of how a shorter TDD pattern does not imply a lower latency. TDD pattern (a) **DDUU**, and (b) **DU**. module built on top of ns-3 [28]. ChronoRAN demonstrates superior performance in both accuracy and computational efficiency compared to these simulators. As illustrated in Fig. 10, ChronoRAN more accurately captures the latency distribution across two representative scenarios. In contrast, both MATLAB and 5G-LENA significantly underestimate the latency range and fail to replicate the actual distribution shape. Beyond accuracy, the computational cost of traditional simulators is prohibitive. For example, simulating the transmission of 10 000 packets for a single configuration—which takes 16.8 min in a real testbed—required a few minutes in 5G-LENA and MATLAB. In contrast, ChronoRAN computes the full latency distribution in just 2 ms—making it three orders of magnitude faster than 5G-LENA and MATLAB.

E. Need for stochastic framework: We evaluate the importance of random variables (RVs) for the determination of latency. We do so by showing the difference in the latency of the packets when we model the UE preparation time (l_1) and gNB processing time (p_4) with and without RVs. In Fig. 11, we observe that the distribution of the latency of the packets is different when we model the l_1 and p_4 with RVs. The Wasserstein distance between the model and Real-World is 0.056 when we do not model the RVs and 0.027 when we do, which is a significant improvement.

F. Configuration Optimizer: For the sub-6 GHz band with Grant-Based configuration, which we use as a representative case, the optimizer explores a search space of 32 billion possible combinations, as discussed in §4.3. After pruning, the search space shrinks dramatically to 698.8 thousand combinations, and the optimizer can identify the optimal configuration in 45 s, running on a single Intel W-2225 CPU.

The optimizer also gives meaningful insights into the non-monotonicity nature of the problem. For example, we ran the optimizer under numerology 2 (0.25 ms) and radio latency of 450 μ s. Intuitively, one would expect that the shortest TDD period with 2 slots (**DU**) would result in the lowest uplink latency as the UE has more frequent opportunities to transmit on the uplink. However, contrary to intuition, optimizing for the TDD and SR periods, the optimizer selects

4 slots in a TDD period (**DDUU**). The average latency of the 4 slots TDD period, reported by the optimizer is 2.01 ms with min and max latency of 1.67 ms and 2.47 ms. Running the model for the 2 slots TDD period would result in 2.7 ms, 2.95 ms, and 3.2 ms for min, average, and max respectively, which is higher than the optimal case. To better understand why, consider the example in Fig. 12. Since the gNB and UE need to submit the RF samples a few slots in advance (a_1 & k_2 in the figure) to give the radio enough time to prepare and transmit these samples, both the UL grant and the data are delayed when using the shorter TDD pattern (**DU**).

G. Possible URLLC Configurations: Leveraging ChronoRAN, we can obtain the latency variation across all possible configurations. This enables us to evaluate 1) whether a given latency can be achieved with specific system conditions and 2) the proportion of configurations that can achieve a given latency with a specified reliability. Such capabilities empower network operators to assess the system’s inherent bottlenecks while selecting the most suitable hardware combinations and support service providers in designing URLLC-oriented devices to meet the latency requirements.

We present the number of configurations able to achieve a given latency with a given reliability in Tab. 1 when using a radio unit with radio latency 450 μ s (similar to our testbed). Since the goal of this analysis is to evaluate all possible configurations, we leverage the Ray framework to parallelize the optimizer across 14 machines, significantly increasing the available computational power. Out of all configurations, none can reliably go below 1 ms in FR1 using grant-based access. In FR2 (mmWave), no configuration can achieve sub 0.5 ms latencies without resorting to Grant-Free access. Grant-Based transmission struggles to meet stringent latency targets, with no configurations achieving 0.5 ms and some meeting 1 ms. In contrast, Grant-Free access offers improved latency performance, with up to 11.58 % of configurations in FR1 and 19.37 % in FR2 achieving 2 ms latency at 50 % reliability. Nevertheless, increasing reliability constraints significantly reduces the number of feasible configurations, particularly for Grant-Based schemes. This emphasizes that achieving high reliability remains a challenge.

Finally, an important insight that ChronoRAN gives us is that simply reducing the numerology (slot duration) is not enough to achieve URLLC, an assumption made by several prior works [20, 33, 66, 74]. Fig. 9 shows how the uplink latency varies versus numerologies, given an average radio preparation time of 0.5 ms and average UE and gNB processing times of 1.46 ms and 0.4 ms. While the results indicate that latency decreases as the numerology increases, other sources of latency quickly become the bottleneck, and increasing the numerology does not help. Using this setup,

Reliability [%]	Grant-Based			Grant-Free		
	50	90	99.99	50	90	99.99
FR1	0.5 ms	0	0	0	0	0
	1 ms	0	0	13.7M	3.2M	3.2M
	2 ms	9.3k	0	37.2M	16.4M	12.2M
FR2	0.5 ms	0	0	165.0M	8.9M	8.9M
	1 ms	0	0	829.4M	255.1M	203.7M
	2 ms	183.9M	60.3M	43.8M	2.0B	983.4M
						692.1M

Table 1: Percentage of configurations achieving a given latency reliability target under *non-negligible radio latency*. Tested valid configurations (after pruning): 326.6M (FR1) and 11.8B (FR2).

even with the highest numerology, the URLLC requirement (0.5 ms for UL transmission) remains unachievable.

7 RELATED WORK

Latency Analysis. Latency modeling and analysis in 5G have been explored in recent years [15, 43, 51, 52, 58, 63, 68, 78]. However, these works either use oversimplified models or simply present an analysis based on observed measurements or simulations. For example, [15] and [63] excluded critical system components such as frame structures and hardware overheads. [52] focused exclusively on the 5G uplink scheduling mechanism and was limited to simulation-based evaluations. [78] ignores the system’s inherent bottlenecks and simply assumes that the latency decreases linearly with the time slot duration. Unlike previous works, we propose a comprehensive mathematical model that accurately characterizes latency distributions and captures the complex interactions among critical system components. We also compare experimentally with two of these past works [52, 78] to show that they severely underestimate the latency in §6.

Latency Optimization. Previous studies address the challenges of optimizing latency by modifying protocols and slot configurations. For instance, Nokia [12] emphasizes the need for slotted MAC, central scheduling, and synchronization for deterministic latency. Additionally, [33] discusses avoiding retransmissions to minimize latency, assuming inherent end-to-end latency within a few milliseconds. Comprehensive reviews such as [10, 17, 19, 20, 49, 53, 66] survey enabling technologies for URLLC but often overlook real-world constraints, focusing instead on idealized scenarios. For instance, either negligible processing [17, 20] or protocol-based latencies [20] are assumed. Finally, a lot of research on scheduling algorithms for URLLC, such as in [11, 26, 32, 38, 54, 65, 75], focuses on managing URLLC packets alongside other services, assuming low-latency communication for a single UE and addressing scalability. Finally, [68] proposes sending scheduling requests in advance to reduce latency, an approach that is complementary to our work.

Latency Measurements: Fezeu et al. [21] evaluate the latency of several commercial mmWave implementations, achieving sub-millisecond round trip latency under optimal conditions. However, they note that sub-millisecond latency is only achieved in 4.4 % of packets, severely violating the reliability constraint. In the sub-6 GHz bands, Wirth et al. [74] propose a PHY layer solution for 5G that achieves low latency. However, since this work predates the 5G standards, it does not incorporate the standard specifications, particularly those concerning scheduling and protocol latency, which can significantly increase the overall latency. Joint work by Nokia and Sennheiser focusing on professional audio applications [45] achieves a minimum DL latency of approximately 0.8 ms for a single UE, going higher in steps of 0.5 ms in case of retransmission. This work, however, only supports single-user point-to-point communication using a hardware-accelerated platform, of which the scalability is limited.

Additional empirical works, conduct latency evaluations in real-world campus networks [36, 57, 58] or testbeds [18, 55]: Rischke et al. [57, 58] report Round-Trip-Times (RTTs) between 12 and 40 ms, and evaluate one-way latencies ranging from 2 to 8 ms. Lackner et al. [36] find RTT latencies of 6 to 12 ms, varying significantly with different UEs. Additional work from Qualcomm [55] indicates mmWave URLLC latencies of 1.9 ms for DL and 4.0 ms for UL. Finally, Ericsson [18] demonstrate a use case for industrial automation with robots, achieving a 5 ms latency.

8 DISCUSSION & LIMITATIONS

ChronoRAN is the first framework that formally analyzes and mathematically models 5G RAN latency across a broad range of scenarios. It also provides insight into how 5G networks can be designed and configured to support URLLC. However, we note some limitations and extensions:

- *Scheduling Algorithms & Contention:* We mainly modeled contention assuming a round robin scheduling algorithm. This, however, can be extended to other scheduling algorithms by modifying the scheduling policy and following the same logic as §E.8, which is beyond the scope of our paper.
- *Wireless Channel:* Our current model and implementation of ChronoRAN do not account for wireless channel quality and packet retransmission at MAC or RLC layers. The focus of ChronoRAN is on analyzing latency bottlenecks and configuration trade-offs under favorable channel conditions. The impact of the wireless channel on URLLC reliability has been studied in prior work [67, 71]. While ChronoRAN could be extended to incorporate wireless channel models, we leave such extension to future work.
- *Power Saving Modes:* Power saving modes (e.g., DRX) can introduce significant initial latency (up to 300 ms in our tests on MNO) after long inactivity periods. ChronoRAN currently

does not model these modes. However, the model could be extended by tracking on/off durations, similarly to how SR periods are handled, and incorporating the resulting waiting time into latency calculations. In practice, power saving modes are typically disabled for URLLC, and in our experiments on *MNO*, the UE entered power saving mode only after at least 10 s of inactivity.

REFERENCES

- [1] 3GPP. 2017. *NR; NR and NG-RAN Overall description; Stage-2*. Technical Report 3GPP TS 38.300 version 1.1.1 Release 15. 3GPP. https://www.3gpp.org/ftp/Specs/archive/38_series/38.300/38300-111.zip
- [2] 3GPP. 2019. *Study on physical layer enhancements for NR ultra-reliable and low latency case (URLLC)*. Technical Report 3GPP TR 38.824 version 16.0.0 Release 16. 3GPP. https://www.3gpp.org/ftp/Specs/archive/38_series/38.824/38824-g00.zip
- [3] 3GPP. 2020. *Physical layer procedures for data*. Technical Report 3GPP TS 38.214 16.2.0 Release 16. 3GPP. https://www.etsi.org/deliver/etsi_ts/138200_138299/138214/16.02.00_60/ts_138214v160200p.pdf
- [4] 3GPP. 2022. *5G; NR; User Equipment (UE) radio transmission and reception; Part 1: Range 1 Standalone*. Technical Report 3GPP TS 38.101-1 version 17.5.0 Release 17. 3GPP. https://www.etsi.org/deliver/etsi_ts/138100_138199/138101/17.05.00_60/ts_138101v170500p.pdf
- [5] 3GPP. 2023. *User Equipment (UE) radio transmission and reception; Part 1: Range 1 Standalone*. Technical Report 3GPP TS 38.101-1 version 17.8.0 Release 17. 3GPP. https://www.etsi.org/deliver/etsi_ts/138100_138199/138101/17.08.00_60/ts_138101v170800p.pdf
- [6] 3GPP. 2024. *5G; NR; Physical channels and modulation*. Technical Report 3GPP TS 38.211 version 18.2.0 Release 18. 3GPP. https://www.etsi.org/deliver/etsi_ts/138200_138299/138211/18.02.00_60/ts_138211v180200p.pdf
- [7] 3GPP. 2024. *5G; Study on scenarios and requirements for next generation access technologies*. Technical Report 3GPP TR 38.913 version 18.0.0 Release 18. 3GPP. https://www.etsi.org/deliver/etsi_tr/138900_138999/138913/18.00.00_60/tr_138913v180000p.pdf
- [8] Aaron Turner. 1999. tcpreplay. <https://tcpreplay.appneta.com/>. [Online; Last accessed: 19-Jan-2025].
- [9] Renato Barbosa Abreu. 2019. Uplink Grant-free Access for Ultra-Reliable Low-Latency Communications in 5G: Radio Access and Resource Management Solutions. PhD supervisor: Prof. Preben Mogenssen, Aalborg University Assistant PhD supervisors: Assoc. Prof. Gilberto Berardinelli, Aalborg University Prof. Klaus Pedersen, Aalborg University.
- [10] Rashid Ali, Yousaf Bin Zikria, Ali Kashif Bashir, Sahil Garg, and Hyung Seok Kim. 2021. URLLC for 5G and Beyond: Requirements, Enabling Incumbent Technologies and Network Intelligence. *IEEE Access* 9 (2021), 67064–67095. <https://doi.org/10.1109/ACCESS.2021.3073806>
- [11] Arjun Anand, Gustavo de Veciana, and Sanjay Shakkottai. 2020. Joint Scheduling of URLLC and eMBB Traffic in 5G Wireless Networks. *IEEE/ACM Transactions on Networking* 28, 2 (2020), 477–490. <https://doi.org/10.1109/TNET.2020.2968373>
- [12] Nihel Benzaoui. 2020. Deterministic Latency Networks for 5G Applications. In *2020 European Conference on Optical Communications (ECOC)*. Institute of Electrical and Electronics Engineers (IEEE), Brussels, Belgium, 1–4. <https://doi.org/10.1109/ECOC48923.2020.9333411>
- [13] Gabriel Brown, P Analyst, and H Reading. 2018. Ultra-reliable low-latency 5G for industrial automation. *Technol. Rep. Qualcomm* 2 (2018), 52065394. <https://www.qualcomm.com/content/dam/qcomm-martech/dm-assets/documents/ultra-reliable-low-latency-5g-for-industrial-automation.pdf>
- [14] Marwa Chafii, Lina Bariah, Sami Muhaidat, and Merouane Debbah. 2023. Twelve Scientific Challenges for 6G: Rethinking the Foundations of Communications Theory. *Commun. Surveys Tuts.* 25, 2 (apr 2023), 868–904. <https://doi.org/10.1109/COMST.2023.3243918>
- [15] Baldomero Coll-Perales, M. Carmen Lucas-Estañ, Takayuki Shimizu, Javier Gozalvez, Takamasa Higuchi, Sergei Avedisov, Onur Altintas, and Miguel Sepulcre. 2023. End-to-End V2X Latency Modeling and Analysis in 5G Networks. *IEEE Transactions on Vehicular Technology* 72, 4 (2023), 5094–5109. <https://doi.org/10.1109/TVT.2022.3224614>
- [16] Underwood Dudley. 2009. *Euler's theorem and function*. Mathematical Association of America, Washington, DC, 37–40. <https://doi.org/10.5948/UPO9780883859186>
- [17] Ericsson. 2017. *5G Techniques for Ultra Reliable Low Latency Communication*. Ericsson. https://wp-files.comsoc.org/cscn-2017/files/2017/08/Janne_Peisa_Ericsson_CSCN2017.pdf
- [18] Ericsson. 2019. *You Need to See Our Dancing Hexapod Demo from MWC*. Ericsson. <https://www.ericsson.com/en/blog/2019/3/dancing-hexapod-demo-a-success-at-mwc>
- [19] Daquan Feng, Lifeng Lai, Jingjing Luo, Yi Zhong, Canjian Zheng, and Kai Ying. 2021. Ultra-reliable and low-latency communications: applications, opportunities and challenges. *Science China Information Sciences* 64, 2 (20 Jan 2021), 120301. <https://doi.org/10.1007/s11432-020-2852-1>
- [20] Daquan Feng, Changyang She, Kai Ying, Lifeng Lai, Zhanwei Hou, Tony Q. S. Quek, Yonghui Li, and Branka Vucetic. 2019. Toward Ultrareliable Low-Latency Communications: Typical Scenarios, Possible Solutions, and Open Issues. *IEEE Vehicular Technology Magazine* 14, 2 (2019), 94–102. <https://doi.org/10.1109/MVT.2019.2903657>
- [21] Rostand A. K. Fezeu, Eman Ramadan, Wei Ye, Benjamin Minneci, Jack Xie, Arvind Narayanan, Ahmad Hassan, Feng Qian, Zhi-Li Zhang, Jaideep Chandrashekar, and Myungjin Lee. 2023. An In-Depth Measurement Analysis of 5G mmWave PHY Latency and Its Impact on End-to-End Delay. In *Passive and Active Measurement: 24th International Conference, PAM 2023, Virtual Event, March 21–23, 2023, Proceedings*. Springer-Verlag, Berlin, Heidelberg, 284–312.
- [22] Chaghan Ge, Zihui Ge, Xuan Liu, Ajay Mahimkar, Yusef Shaqalle, Yu Xiang, and Shomik Pathak. 2023. Chroma: Learning and Using Network Contexts to Reinforce Performance Improving Configurations. In *Proceedings of the 29th Annual International Conference on Mobile Computing and Networking (Madrid, Spain) (ACM MobiCom '23)*. Association for Computing Machinery, New York, NY, USA, Article 42, 16 pages. <https://doi.org/10.1145/3570361.3613256>
- [23] Andres J Gonzalez, Min Xie, Per Hjalmar Lehne, and Pål Grønsund. 2021. Achieving high throughput and low latency with 5g: A real implementation experience. *IEEE Communications Magazine* 59, 10 (2021), 84–90.
- [24] Rajesh Gupta, Dakshita Reebadiya, and Sudeep Tanwar. 2021. 6G-enabled Edge Intelligence for Ultra-Reliable Low Latency Applications: Vision and Mission. *Computer Standards & Interfaces* 77 (2021), 103521. <https://doi.org/10.1016/j.csi.2021.103521>
- [25] Saqib Hakak, Thippa Reddy Gadekallu, Praveen Kumar Reddy Maddikunta, Swarna Priya Ramu, Parimala M, Chamitha De Alwis, and Madhusanka Liyanage. 2023. Autonomous vehicles in 5G and beyond: A survey. *Vehicular Communications* 39 (2023), 100551. <https://doi.org/10.1016/j.vehcom.2022.100551>
- [26] Md. Emdadul Haque, Faisal Tariq, Muhammad R. A. Khandaker, Kai-Kit Wong, and Yangyang Zhang. 2023. A Survey of Scheduling in 5G URLLC and Outlook for Emerging 6G Systems. *IEEE Access* 11 (2023), 34372–34396. <https://doi.org/10.1109/ACCESS.2023.3264592>
- [27] Ananya Hazarika and Mehdi Rahmati. 2023. Towards an Evolved Immersive Experience: Exploring 5G- and Beyond-Enabled Ultra-Low-Latency Communications for Augmented and Virtual Reality. *Sensors*

- 23, 7 (2023), 25 pages. <https://doi.org/10.3390/s23073682>
- [28] Thomas R Henderson, Mathieu Lacage, and George F Riley. 2008. Network simulations with the ns-3 simulator. In *Proceedings of the ACM SIGCOMM 2008 Conference on Data Communication* (Seattle, WA, USA) (SIGCOMM '08). Association for Computing Machinery, New York, NY, USA, 527. <https://conferences.sigcomm.org/sigcomm/2008/papers/p527-hendersonA.pdf>
- [29] Hongxun Hui, Yi Ding, Qingxin Shi, Fangxing Li, Yonghua Song, and Jinyue Yan. 2020. 5G network-based Internet of Things for demand response in smart grid: A survey on application potential. *Applied Energy* 257 (2020), 113972. <https://doi.org/10.1016/j.apenergy.2019.113972>
- [30] Anyscale Inc. 2020. *Ray*. Ray Project, San Francisco, CA, USA. <https://docs.ray.io/>
- [31] The MathWorks Inc. 2025. *5G Toolbox version: R2025a*. MATLAB, Natick, MA, USA. <https://www.mathworks.com/products/5g.html>
- [32] Hyoungju Ji, Sunho Park, Jeongho Yeo, Younsun Kim, Juho Lee, and Byonghyo Shim. 2018. Ultra-Reliable and Low-Latency Communications in 5G Downlink: Physical Layer Aspects. *IEEE Wireless Communications* 25, 3 (2018), 124–130. <https://doi.org/10.1109/MWC.2018.1700294>
- [33] Niklas A. Johansson, Y.-P. Eric Wang, Erik Eriksson, and Martin Hessler. 2015. Radio access for ultra-reliable and low-latency 5G communications. In *2015 IEEE International Conference on Communication Workshop (ICCW)*. IEEE, London, UK, 1184–1189. <https://doi.org/10.1109/ICCW.2015.7247338>
- [34] Leonid V Kantorovich. 1960. Mathematical methods of organizing and planning production. *Management science* 6, 4 (1960), 366–422.
- [35] Benish Sharfeen Khan, Sobia Jangsher, Ashfaq Ahmed, and Arafat Al-Dweik. 2022. URLLC and eMBB in 5G industrial IoT: A survey. *IEEE Open Journal of the Communications Society* 3 (2022), 1134–1163.
- [36] Thorge Lackner, Julian Hermann, Fabian Dietrich, Christian Kuhn, Mario Angos, Johannes L Jooste, and Daniel Palm. 2022. Measurement and comparison of data rate and time delay of end-devices in licensed sub-6 GHz 5G standalone non-public networks. *Procedia CIRP* 107 (2022), 1132–1137.
- [37] Jingya Li, Keerthi Kumar Nagalapur, Erik Stare, Satyam Dwivedi, Shehzad Ali Ashraf, Per-Erik Eriksson, Ulrika Engström, Woong-Hee Lee, and Thorsten Lohmar. 2022. 5G New Radio for Public Safety Mission Critical Communications. *IEEE Communications Standards Magazine* 6, 4 (2022), 48–55. <https://doi.org/10.1109/MCOMSTD.0002.2100036>
- [38] Jing Li and Xing Zhang. 2020. Deep Reinforcement Learning-Based Joint Scheduling of eMBB and URLLC in 5G Networks. *IEEE Wireless Communications Letters* 9, 9 (2020), 1543–1546. <https://doi.org/10.1109/LWC.2020.2997036>
- [39] Ajay Mahimkar, Ashiwan Sivakumar, Zihui Ge, Shomik Pathak, and Karunasish Biswas. 2021. Auric: using data-driven recommendation to automatically generate cellular configuration. In *Proceedings of the 2021 ACM SIGCOMM 2021 Conference (Virtual Event, USA) (SIGCOMM '21)*. Association for Computing Machinery, New York, NY, USA, 807–820. <https://doi.org/10.1145/3452296.3472906>
- [40] Colin L Mallows. 1972. A note on asymptotic joint normality. *The Annals of Mathematical Statistics* 43, 2 (1972), 508–515.
- [41] Mike Muuss. 1983. Ping. <https://github.com/iputils/iputils/tree/master/ping>. [Online; Last accessed: 19-Jan-2025].
- [42] Andrea Moglia, Konstantinos Georgiou, Blagoi Marinov, Evangelos Georgiou, Raffaella Nice Berchiolli, Richard M. Satava, and Alfred Cuschieri. 2022. 5G in Healthcare: From COVID-19 to Future Challenges. *IEEE Journal of Biomedical and Health Informatics* 26, 8 (2022), 4187–4196. <https://doi.org/10.1109/JBHI.2022.3181205>
- [43] Samie Mostafavi, Marius Tillner, Gourav Prateek Sharma, and James Gross. 2024. EDAF: An End-to-End Delay Analytics Framework for 5G-and-Beyond Networks. In *IEEE INFOCOM 2024 - IEEE Conference on Computer Communications Workshops (INFOCOM WKSHPs)*. Institute of Electrical and Electronics Engineers (IEEE), Vancouver, BC, Canada, 1–6. <https://doi.org/10.1109/INFOCOMWKSHPs61880.2024.10620853>
- [44] Navid Nikaein, Mahesh K. Marina, Saravana Manickam, Alex Dawson, Raymond Knopp, and Christian Bonnet. 2014. OpenAirInterface: A Flexible Platform for 5G Research. *SIGCOMM Comput. Commun. Rev* 44, 5 (oct 2014), 33–38. <https://doi.org/10.1145/2677046.2677053>
- [45] Nokia and Sennheiser. 2020. *Low Latency 5G for Professional Audio Transmission*. Nokia and Sennheiser. https://d1p0gxnqcu0lvz.cloudfront.net/documents/Nokia_Low_Latency_5G_for_Professional_Audio_Transmission_White_Paper_EN.pdf Accessed on February 9, 2026.
- [46] European 5G Observatory. 2018. Commercial 5G launches – 5G Observatory. <https://5gobservatory.eu/overview-5g-commercial-launches/> Accessed on February 9, 2026.
- [47] Open5GS. 2017. Open5GS Project: Open source 5G core network. <https://open5gs.org/>. [Online; Last accessed: 17-Jan-2025].
- [48] Victor M Panaretos and Yoav Zemel. 2019. Statistical aspects of Wasserstein distances. *Annual review of statistics and its application* 6, 1 (2019), 405–431.
- [49] Imtiaz Parvez, Ali Rahmati, Ismail Guvenc, Arif I. Sarwat, and Huaiyu Dai. 2018. A Survey on Low Latency Towards 5G: RAN, Core Network and Caching Solutions. *IEEE Communications Surveys & Tutorials* 20, 4 (2018), 3098–3130. <https://doi.org/10.1109/COMST.2018.2841349>
- [50] Natale Patriciello, Sandra Lagen, Biljana Bojovic, and Lorenza Giupponi. 2019. An E2E simulator for 5G NR networks. *Simulation Modelling Practice and Theory* 96 (2019), 101933. <https://doi.org/10.1016/j.simpat.2019.101933>
- [51] Natale Patriciello, Sandra Lagen, Lorenza Giupponi, and Biljana Bojovic. 2018. 5G New Radio Numerologies and their Impact on the End-To-End Latency. In *2018 IEEE 23rd International Workshop on Computer Aided Modeling and Design of Communication Links and Networks (CAMAD)*. Institute of Electrical and Electronics Engineers (IEEE), Barcelona, Spain, 1–6. <https://doi.org/10.1109/CAMAD.2018.8514979>
- [52] Natale Patriciello, Sandra Lagen, Lorenza Giupponi, and Biljana Bojovic. 2019. The Impact of NR Scheduling Timings on End-to-End Delay for Uplink Traffic. In *2019 IEEE Global Communications Conference (GLOBECOM)*. Institute of Electrical and Electronics Engineers (IEEE), Waikoloa, HI, USA, 1–6. <https://doi.org/10.1109/GLOBECOM38437.2019.9013231>
- [53] Petar Popovski, Jimmy J. Nielsen, Cedomir Stefanovic, Elisabeth de Carvalho, Erik Strom, Kasper F. Trillingsgaard, Alexandru-Sabin Bana, Dong Min Kim, Radoslaw Kotaba, Jihong Park, and Rene B. Sorensen. 2018. Wireless Access for Ultra-Reliable Low-Latency Communication: Principles and Building Blocks. *IEEE Network* 32, 2 (2018), 16–23. <https://doi.org/10.1109/MNET.2018.1700258>
- [54] Yerra Prathyusha and Tsang-Ling Sheu. 2022. Coordinated Resource Allocations for eMBB and URLLC in 5G Communication Networks. *IEEE Transactions on Vehicular Technology* 71, 8 (2022), 8717–8728. <https://doi.org/10.1109/TVT.2022.3176018>
- [55] Qualcomm. 2020. *Making 5G NR a Reality*. Technical Report. Qualcomm. https://www.qualcomm.com/content/dam/qcomm-martech/dm-assets/documents/powerpoint_presentation_-_making_5g_nr_a_reality_february_2020_web.pdf
- [56] Qualcomm. 2021. *Qualcomm Snapdragon X65 5G Modem-RF System*. <https://www.qualcomm.com/products/snapdragon-x65-5g-modem-rf-system> [Online; Last accessed: 31-Jan-2025].
- [57] Justus Rischke, Peter Sossalla, Sebastian Itting, Frank HP Fitzek, and Martin Reisslein. 2021. 5G campus networks: A first measurement study. *IEEE Access* 9 (2021), 121786–121803.

- [58] Justus Rischke, Christian Vielhaus, Peter Sossalla, Sebastian Itting, Giang T. Nguyen, and Frank H. P. Fitzek. 2022. Empirical Study of 5G Downlink & Uplink Scheduling and its Effects on Latency. In *2022 IEEE 23rd International Symposium on a World of Wireless, Mobile and Multimedia Networks (WoWMoM)*. Institute of Electrical and Electronics Engineers (IEEE), Belfast, United Kingdom, 11–19. <https://doi.org/10.1109/WoWMoM54355.2022.00017>
- [59] Roland Schemers. 1992. fping. <https://fping.org/>. [Online; Last accessed: 19-Jan-2025].
- [60] P1 Security. 2024. QCSuper release 2.0.1. <https://github.com/P1sec/QCSuper>.
- [61] William Sentosa, Balakrishnan Chandrasekaran, P. Brighten Godfrey, Haitham Hassanieh, and Bruce Maggs. 2023. DChannel: Accelerating Mobile Applications With Parallel High-bandwidth and Low-latency Channels. In *20th USENIX Symposium on Networked Systems Design and Implementation (NSDI 23)*. USENIX Association, Boston, MA, 419–436. <https://www.usenix.org/conference/nsdi23/presentation/sentosa>
- [62] Changyang She and Yonghui Li. 2024. *Ultra-Reliable and Low-Latency Communications in 6G: Challenges, Solutions, and Future Directions*. Springer International Publishing, Cham, 27. https://doi.org/10.1007/978-3-031-37920-8_24
- [63] Marco Skocaj, Francesca Conserva, Nicol Sarcone Grande, Andrea Orsi, Davide Micheli, Giorgio Ghinamo, Simone Bizzarri, and Roberto Verdone. 2023. Data-driven Predictive Latency for 5G: A Theoretical and Experimental Analysis Using Network Measurements. In *2023 IEEE 34th Annual International Symposium on Personal, Indoor and Mobile Radio Communications (PIMRC)*. Institute of Electrical and Electronics Engineers (IEEE), London, UK, 1–6. <https://doi.org/10.1109/PIMRC56721.2023.10293861>
- [64] Software Radio Systems. 2022. srsRAN Project: Open source RAN. <https://www.srsran.com/>. [Online; Last accessed: 17-Jan-2025].
- [65] Rana M. Sohaib, Oluwakayode Onireti, Yusuf Sambo, Rafiq Swash, Shuja Ansari, and Muhammad A. Imran. 2023. Intelligent Resource Management for eMBB and URLLC in 5G and Beyond Wireless Networks. *IEEE Access* 11 (2023), 65205–65221. <https://doi.org/10.1109/ACCESS.2023.3288698>
- [66] Gordon J. Sutton, Jie Zeng, Ren Ping Liu, Wei Ni, Diep N. Nguyen, Bee-shanga A. Jayawickrama, Xiaojing Huang, Mehran Abolhasan, Zhang Zhang, Eryk Dutkiewicz, and Tiejun Lv. 2019. Enabling Technologies for Ultra-Reliable and Low Latency Communications: From PHY and MAC Layer Perspectives. *IEEE Communications Surveys & Tutorials* 21, 3 (2019), 2488–2524. <https://doi.org/10.1109/COMST.2019.2897800>
- [67] Michal Sybis, Krzysztof Wesolowski, Keeth Jayasinghe, Venkatkumar Venkatasubramanian, and Vladimir Vukadinovic. 2016. Channel Coding for Ultra-Reliable Low-Latency Communication in 5G Systems. In *2016 IEEE 84th Vehicular Technology Conference (VTC-Fall)*. IEEE, Montreal, QC, Canada, 1–5. <https://doi.org/10.1109/VTCTFall.2016.7880930>
- [68] Zhaowei Tan, Jinghao Zhao, Yuanjie Li, Yifei Xu, and Songwu Lu. 2021. Device-Based LTE Latency Reduction at the Application Layer. In *18th USENIX Symposium on Networked Systems Design and Implementation (NSDI 21)*. USENIX Association, 471–486. <https://www.usenix.org/conference/nsdi21/presentation/tan>
- [69] Talal Touseef, William Sentosa, Milind Kumar Vaddiraju, Debopam Bhattacharjee, Bala Chandrasekaran, P. Brighten Godfrey, and Shubham Tiwari. 2023. Boosting Application Performance using Heterogeneous Virtual Channels: Challenges and Opportunities. In *22nd ACM Workshop on Hot Topics in Networks (HotNets)*. ACM, Cambridge MA USA, 139 – 146. <https://doi.org/10.1145/3626111.3628193>
- [70] Mikko Uitto and Antti Heikkinen. 2021. Evaluation of live video streaming performance for low latency use cases in 5g. In *2021 Joint European Conference on Networks and Communications & 6G Summit (EuCNC/6G Summit)*. IEEE, IEEE, Porto, Portugal, 431–436.
- [71] Sutharshun Varatharaajan, Marcus Grossmann, and Giovanni Del Galdo. 2022. 5G New Radio Physical Downlink Control Channel Reliability Enhancements for Multiple Transmission-Receiver Point Communications. *IEEE Access* 10 (2022), 97394–97407. <https://doi.org/10.1109/ACCESS.2022.3206027>
- [72] Leonid Nisonovich Vaserstein. 1969. Markov processes over denumerable products of spaces, describing large systems of automata. *Problemy Peredachi Informatsii* 5, 3 (1969), 64–72.
- [73] Mojca Volk and Janez Sterle. 2021. 5G Experimentation for Public Safety: Technologies, Facilities and Use Cases. *IEEE Access* 9 (2021), 41184–41217. <https://doi.org/10.1109/ACCESS.2021.3064405>
- [74] Thomas Wirth, Matthias Mehlhose, Jens Pilz, Bernd Hofeld, and Dennis Wieruch. 2016. 5G new radio and ultra low latency applications: A PHY implementation perspective. In *2016 50th Asilomar Conference on Signals, Systems and Computers*. IEEE, Pacific Grove, CA, USA, 1409–1413. <https://doi.org/10.1109/ACSSC.2016.7869608>
- [75] Hao Yin, Lyutianyang Zhang, and Sumit Roy. 2021. Multiplexing URLLC Traffic Within eMBB Services in 5G NR: Fair Scheduling. *IEEE Transactions on Communications* 69, 2 (2021), 1080–1093. <https://doi.org/10.1109/TCOMM.2020.3035582>
- [76] Mingyang Zhang, Haohao Fu, Yong Li, and Sheng Chen. 2019. Understanding Urban Dynamics From Massive Mobile Traffic Data. *IEEE Transactions on Big Data* 5, 2 (2019), 266–278. <https://doi.org/10.1109/TBDATA.2017.2778721>
- [77] Shunqing Zhang, Xiuqiang Xu, Yiqun Wu, and Lei Lu. 2014. 5G: Towards energy-efficient, low-latency and high-reliable communications networks. In *IEEE International Conference on Communication Systems, ICCS 2014, Macau, China, November 19-21, 2014*. IEEE, Macau, China, 197–201. <https://doi.org/10.1109/ICCS.2014.7024793>
- [78] Yong Zhao and Weiliang Xie. 2023. Physical Layer Round Trip Latency Analysis and Estimation for 5G NR. In *2023 International Wireless Communications and Mobile Computing (IWCMC)*. Institute of Electrical and Electronics Engineers (IEEE), Marrakesh, Morocco, 971–976. <https://doi.org/10.1109/IWCMC58020.2023.10183295>

A PROOFS

A.1 Proof of lemma 4.1

PROOF. We solve this problem using Euler’s theorem [16] in number theory.

Based on Eq. (3), for $x \in A$, $y \in B$, we can write:

$$SR_O + x \cdot SR_P \equiv_T y \implies x \cdot \frac{SR_P}{n} \equiv_T \frac{y - SR_O}{n} \quad (18)$$

Based on Euler’s theorem we can deduce (φ is Euler’s totient function):

$$n \mid y - SR_O \quad (19)$$

$$x \equiv_T \frac{y - SR_O}{n} \cdot \left(\frac{SR_P}{n} \right)^{\varphi\left(\frac{T}{n}\right)-1} \quad (20)$$

From Eq. (4), we know that if $y \in B$, then:

$$y \subseteq \{d + 1, \dots, T - 1\} \quad (21)$$

We define set C as the largest set of integers satisfying Eq. (19) and Eq. (21). For any $z \in C$, we can write:

$$n \mid (z - SR_O) \iff \exists a \in \mathbb{N}, \quad y = n \cdot a + SR_O \quad (22)$$

$$\implies d + 1 \leq n \cdot a + SR_O \leq T - 1 \quad (23)$$

$$\iff \frac{d + 1 - SR_O}{n} \leq a \leq \frac{T - 1 - SR_O}{n}. \quad (24)$$

Reliability [%]	Grant-Based			Grant-Free		
	50	90	99.99	50	90	99.99
0.5 ms	0	0	0	0	0	0
FR1 1 ms	0	0	0	15.3M	3.7M	3.7M
2 ms	60.3k	0	0	40.7M	18M	13.3M
0.5 ms	0	0	0	356.6M	9.8M	9.8M
FR2 1 ms	19.7M	0	0	1.6B	469.2M	396M
2 ms	1.1B	496.0M	409.0M	3.7B	2.0B	1.4B

Table 2: Number of configurations achieving a given latency reliability target under *negligible radio latency*. Tested valid configurations (after pruning): 351.3M (FR1) and 19.1B (FR2).

Consequently, if we define set D as follows:

$$D = \begin{cases} \left\{ \left\lfloor \frac{d+1-SR_O}{n} \right\rfloor, \dots, \left\lfloor \frac{T-1-SR_O}{n} \right\rfloor \right\}; & \text{if } \left\lfloor \frac{d+1-SR_O}{n} \right\rfloor < \left\lfloor \frac{T-1-SR_O}{n} \right\rfloor \\ \emptyset; & \text{otherwise.} \end{cases}$$

C can be written as: $C = \{n \cdot j + SR_O \mid j \in D\}$ (25)

Next, we aim to prove that $B = C$. We must show $B \subseteq C$ and $C \subseteq B$. We already know $B \subseteq C$ because any $y \in B$ satisfies Eq. (19) and Eq. (21), and C is the largest set of integers meeting these conditions. To show $C \subseteq B$, we must demonstrate that for every $z \in C$, there exists an $x \in A$ such that Eq. (18) holds. We can find this x by defining it as in Eq. (20); hence, we have proved that:

$$B = C = \{n \cdot j + SR_O \mid j \in D\} \quad (26)$$

Now that we have found B , we can find A by substituting all members of B as y in Eq. (20), and finding all corresponding x . For each $y \in B$ there are exactly n corresponding $x \in \{1, \dots, T\}$, which can be written as follows after substitution:

$$A = \left\{ \left(j \cdot \left(\frac{SR_P}{n} \right)^{\varphi\left(\frac{T}{n}\right)-1} \bmod \frac{T}{n} \right) + \frac{T}{n} i \mid j \in D, i \in \{0, \dots, n-1\} \right\}$$

□

B ADDITIONAL RESULTS

B.1 Model and Configuration Optimizer Evaluation

We present latency distributions for additional scenarios in Fig. 13. Fig. 14 and Fig. 15 show the corresponding latency bounds and Wasserstein distances for these scenarios.

Moreover, we present results analogous to those in Tab.1, but obtained using a more ideal radio unit with a radio latency of 50 μ s, as shown in Tab.2. We observe that significantly more configurations satisfy the URLLC requirements, particularly in FR2. This is primarily because, in FR1, the longer slot durations introduce substantial additional transmission latency. Overall, these results highlight the trade-offs among latency, reliability, and access schemes.

B.2 Traffic Generation

To validate ChronoRAN against latency measurements across diverse traffic patterns, we generate and send traffic using various arrival and inter-arrival distributions and packet sizes. Existing tools such as ping [41], fping [59], and tcpreplay [8] lack the required accuracy, so we built a custom C-based traffic generator. Unlike general-purpose tools that trade precision for memory efficiency, our tool precomputes and stores packets with timestamps, then transmits them in a lightweight loop. This reduces inter-arrival jitter at the cost of memory efficiency, which is acceptable as we only use this to validate the accuracy of ChronoRAN. We further improve accuracy by raising process priority, pinning it to a dedicated core, and using expiration-based timers. We evaluate their performance on an Intel Xeon W-2225 with 64 GB RAM running Linux 6.8.0-50-lowlatency. Our tool consists of two components: a *generator* and a *replayer*. The generator produces packets with Gaussian, Poisson, or constant inter-arrival times, while the replayer reproduces traces with high fidelity.

To assess precision, we generated 10 000 packets with a constant 40 ms interval using our generator, ping [41], and fping [59]. As shown in Fig. 16a, our tool achieves the narrowest distribution, centered on the target interval. The standard deviation is only 0.01 ms, compared to 0.16 ms and 0.13 ms for ping and fping, respectively. Finally, Fig. 16b and 16c demonstrate the ability to accurately generate Gaussian and Poisson traffic with varying parameters.

C CONFIGURATION OPTIMIZER

We provide the configuration variables used in §6F to evaluate the performance of ChronoRAN's configuration optimizer. Taking the Cartesian product of these variables yields approximately 32.7 billion possible combinations.

```

1 ue_preparation_time_sr_mean: {value: 1.464, optimize: false} #
  ms
2 ue_preparation_time_sr_std: {value: 0.175, optimize: false} #
  ms
3 gnb_processing_time_sr: {value: 0.1, optimize: false} # ms
4 mac_scheduling_time: {value: 0.1, optimize: false} # ms
5 gnb_phy_processing_time: {value: 0.01, optimize: false} # ms
6 radio_preparation_time: {value: 0.5, optimize: false} # ms
7 ue_l2_down_processing_time: {value: 0.3, optimize: false} # 0.6
  # ms
8 gnb_processing_time_l1_up_mean: {value: 0.13, optimize: false}
  # ms
9 gnb_processing_time_l1_up_std: {value: 0.40, optimize: false} #
  ms
10 gnb_processing_time_l1_up_loc: {value: 0.27, optimize: false} #
  ms
11 slot_duration: {value: 0.5, optimize: true, discrete_values:
  [0.25, 0.5, 1.0]} # ms
12 dl_ul_tx_period: {value: 4, optimize: true, discrete_values:
  [2, 4, 5, 6, 8, 10, 12, 16, 20, 40, 80, 160, 320]} # slots
13 nof_dl_slots: {value: 2, optimize: true, discrete_values: [1,
  2, ..., 80]} # slots
14 no_mixed_slot: {value: true, optimize: false}
15 k2: {value: 1, optimize: true, discrete_values: [1, 2, ...,
  16]} # slots
16 sr_period: {value: 4, optimize: true, discrete_values: [1, 2,
  4, 5, 8, 10, 16, 20, 40, 80, 160, 320, 640]} # slots
17 sr_offset: {value: 3, optimize: true, discrete_values: [0, 1,
  ..., 79]} # slots

```

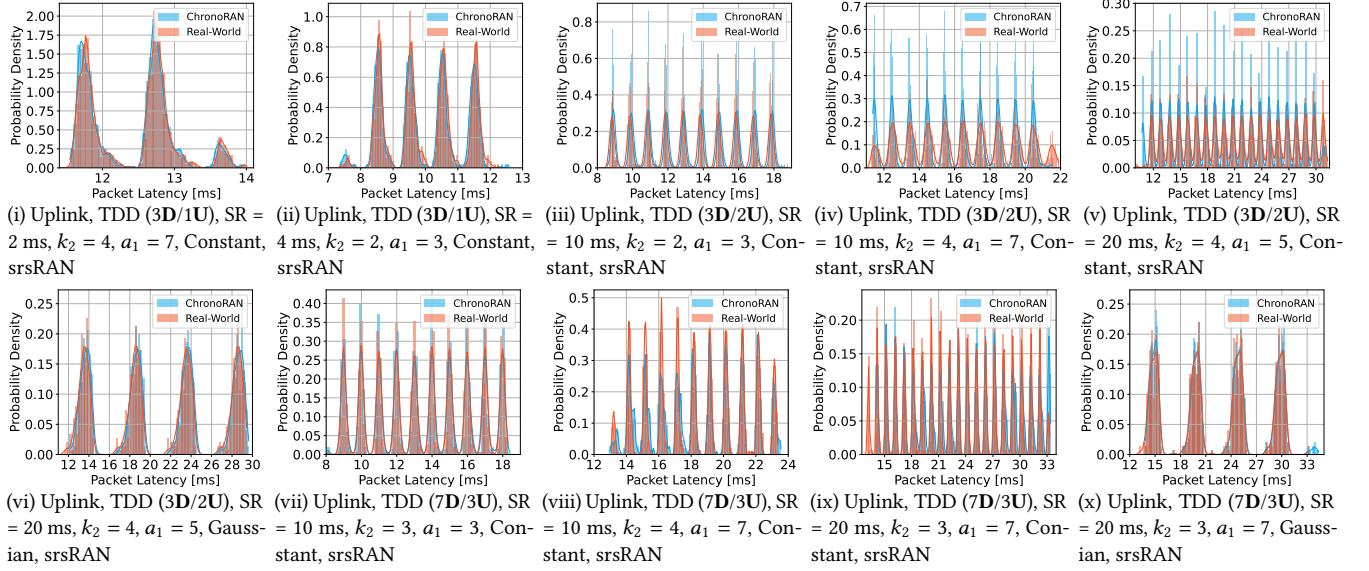


Figure 13: Latency distributions for additional scenarios. We generate traffic using different inter-arrival distributions and packet sizes: 1) Constant – Packets of 64 bytes with a fixed inter-arrival time of 101 ms. 2) Gaussian – Packets of 64 bytes with a Gaussian inter-arrival distribution (mean: 105 ms, standard deviation: 0.05).

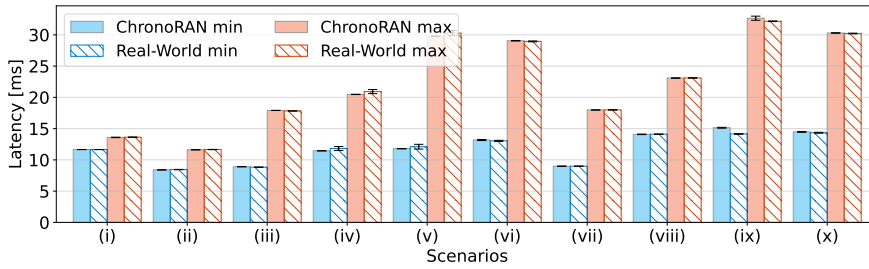


Figure 14: 95th percentile latency bounds comparing ChronoRAN and Real-World under the same scenarios as Fig. 13. Bands show 1 percentile variation.

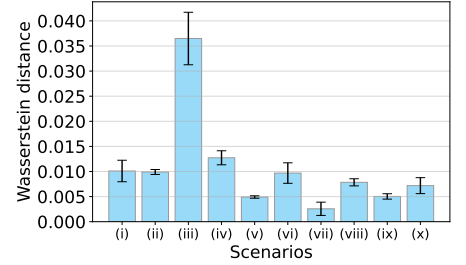


Figure 15: Wasserstein distances of ChronoRAN and Real-World.

```

18 pucch_st_sym: {value: 13, optimize: true, discrete_values: [0,
19 1, ..., 13]} # symbol
19 pucch_nof_sym: {value: 1, optimize: true, discrete_values: [1,
20 2, 3]} # number
20 pdcch_nof_sym: {value: 1, optimize: true, discrete_values: [1,
21 2, 3]} # number
21 in_advance_submission: {value: 1, optimize: true,
discrete_values: [0, 1, 2, 3, 4]} # slots
    
```

D MNO PARAMETERS

We provide the most important parameters used to run ChronoRAN for MNO in Tab.3. We mark each as either directly obtained by decoding RRC messages or learned as explained in §5.

E MODELING THE LATENCY FOR THE REMAINING SCENARIOS

As discussed in Sec. 2 and 3, and as mathematically modeled in Sec. 4.1, our initial analysis concentrated on a Small-Sized

Parameter	Value	Source
TDD Pattern	4D/1U	RRC Message
Numerology (μ)	1	RRC Message
SR Period	20 ms	RRC Message
Radio Latency	< 250 μ s	Learned
a_1	1	Learned
Wired Delay Mean	5.5 ms	Learned
Wired Delay Std Dev	0.8 ms	Learned

Table 3: MNO parameters.

(Size 1) packets in a 5G network. If we define the size of initial grant as g_I bytes, which is determined by network configuration, the formal definition of small packet is as follows.

$$P < g_I \tag{27}$$

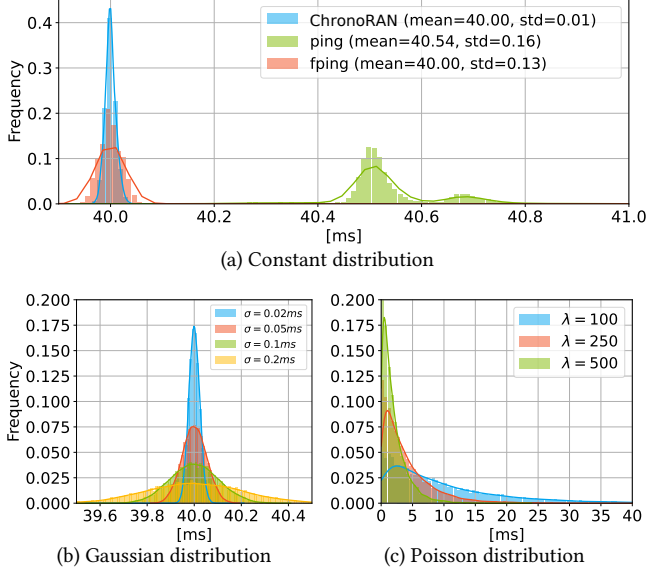


Figure 16: Inter-arrival time of generated packets

This means that the packet is smaller than the initial grant size, and it can be transmitted using the initial grant. In this appendix we thoroughly model and discuss all the remaining scenarios. We discuss larger packets, UL latency for a train of packets, UL and DL latency with TDD Mini-Slot configuration, UL latency with Grant-Free access, DL latency in TDD, and frequency-division duplexing (FDD) configurations.

We classify the various scenarios as follows, and provide the corresponding mathematical modeling for each case. In order to reuse the formulation in § 4.1, we summarize the section in Pseudocode 1.

Pseudocode 1 Total Latency of TDD UL for Size 1 Packets

- 1: Initialize $o_1 \leftarrow t_{arrival}$ where $t_{arrival}$ is the arrival time of the packet.
 - 2: Calculate w_1 using Eq. (2) to Eq. (7).
 - 3: Calculate w_2 using Eq. (8).
 - 4: Calculate w_3 using Eq. (9) to Eq. (13).
 - 5: Calculate w_4 using Eq. (14).
 - 6: Calculate w_5 using Eq. (15) to Eq. (17).
 - 7: Calculate w_6 using Eq. (28).
 - 8: Calculate w_7 using Eq. (28).
 - 9: Calculate $Total_{Latency}$ using Eq. (1).
 - 10: **return** $w_1, w_2, w_3, w_4, w_5, w_6, w_7, Total_{Latency}$
-

E.1 UL Latency for Size 2 packets in TDD

Consider the case where a UE transmits a packet larger than the initial grant size, i.e., Eq. (27) no longer holds. The packet's journey is shown in Fig. 17 for a *TDD Common Configuration* with the **DDUU** pattern. The first steps mirror those of the ping packet in § 3: the UE sends a scheduling

request after w_1 , receives the initial grant after w_3 , and transmits data after w_5 . The difference arises because the packet exceeds the initial grant, which is typically small and mainly intended for buffer status reporting (②). Using this grant, the UE sends g_I bytes of data and a report showing the remaining bytes in its buffer. This report is known as the Buffer Status Report (BSR) ⁶ (③). The gNB uses this information to allocate additional resources to the UE in the next UL slots. Unlike SR, which is sent on PUCCH and processed at the start of the uplink slot (①), the BSR is carried on PUSCH and only processed in the subsequent slot (④).

The variables w_1 - w_7 are defined and computed as in § 4.1. Specifically, we had the following.

$$w_6 = S, \quad w_7 = p_4 \quad (28)$$

Once the gNB receives the BSR, we introduce additional variables to capture the extra latency, as illustrated in Fig. 17.

w'_3 : Time between the gNB receiving the BSR and sending a new grant. Unlike the initial grant, this allocation carries the remaining packet data.

w'_5 : Time from the slot carrying the new grant to the uplink slot where the UE transmits using it.

w'_6 : Transmission time of data on granted uplink slots within a TDD period.

Modeling of w'_3 : As in § 4.1, the gNB requires p_1 seconds to process UL samples, decoding symbol by symbol. Since scheduling starts at slot boundaries, the last symbol dominates processing time, adding p_1 . The MAC processing and grant scheduling can be expressed as:

$$\text{Start of MAC Processing} = o_1 + w_1 + w_3 + w_5 + w_6 + \left\lceil \frac{p_1}{S} \right\rceil S \quad (29)$$

$$\text{Scheduled Slot for Grant} = \frac{o_1 + w_1 + w_3 + w_5 + w_6}{S} + \left\lceil \frac{p_1}{S} \right\rceil + a_1 + 1 \quad (30)$$

Thus,

$$re'_1 \equiv_T \frac{o_1 + w_1 + w_3 + w_5 + w_6}{S} + \left\lceil \frac{p_1}{S} \right\rceil + a_1 + 1 \quad (31)$$

$$w'_3 = \begin{cases} \left(\left\lceil \frac{p_1}{S} \right\rceil + a_1 + 1 \right) S, & re'_1 \leq d; \\ \left(\left\lceil \frac{p_1}{S} \right\rceil + a_1 + 1 + (T - re'_1) \right) S, & \text{otherwise.} \end{cases} \quad (32)$$

Modeling of w'_5 : Similar to w_5 , but with potentially larger UL data, so the UE might need more time to prepare. We define l'_2 as the time for the UE to prepare samples after the grant. Then,

$$k'_{2min} = \left\lceil \frac{w_4 + l'_2}{S} \right\rceil, \quad k'_{2min} \leq k_2 \quad (33)$$

Minimizing k_2 gives:

$$re'_2 \equiv_T \frac{o_1 + w_1 + w_3 + w_5 + w_6 + w'_5}{S} + k'_{2min} \quad (34)$$

⁶The BSR is very small (less than a byte), so we neglect its contribution to the grant size.

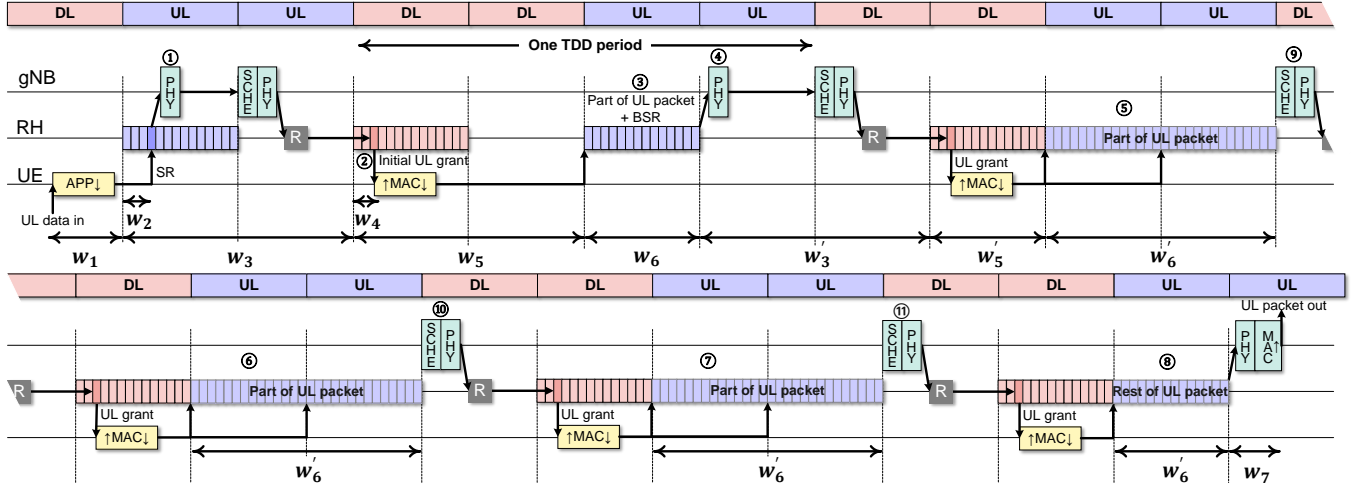


Figure 17: Journey of a packet for larger packets. A TDD Common Configuration with the DDUU pattern is used.

$$k_2 = \begin{cases} k'_{2\min}, & re'_2 \geq d; \\ k'_{2\min} + d - re'_2, & \text{otherwise.} \end{cases} \quad (35)$$

$$w'_5 = k_2 S \quad (36)$$

Modeling of w'_6 : By definition, w'_6 is the transmission time over contiguous UL slots within one TDD period. If the packet spans multiple periods (⑤–⑧ in Fig. 17), w'_6 accounts for all. In this example we assume a single UE (although we also model multi-UE in §E.8), so all available UL resources are allocated. The number of required UL slots is determined by the maximum bytes per slot, computed later in this section.

The bytes per uplink (UL) slot depend on (i) the bandwidth and subcarrier spacing (SCS), and (ii) the modulation and coding scheme (MCS). In 5G, a resource block (RB) spans 12 subcarriers in frequency and 14 symbols in time. The number of RBs for each bandwidth/SCS pair is prescribed in the standard [5]. The MCS, determined by channel quality, specifies modulation order Q_m and coding rate R . The mapping between them is also prescribed in the standard [3]. Since SCS is tied to slot duration T (which is uniquely determined from SCS), we write $N_{RB}[B, T]$ for the RB count at bandwidth B and slot duration T . Given MCS index I_{MCS} , $Q_m[I_{MCS}]$ and $R[I_{MCS}]$ are obtained from the tables in the standard [3]. The maximum payload per UL slot (excluding control) is defined and calculated as follows.

$$Bi_{UL} = N_{RB}[B, T] \cdot 12 \cdot Q_m[I_{MCS}] \cdot R[I_{MCS}] \cdot (14 - UC_{no}) \quad (37)$$

After receiving the BSR, the gNB records the buffer status and allocates resources until the buffer is empty, updating it only upon new BSRs. Here we assume a single big packet in the buffer, so no further BSRs are sent (multi-packet arrivals are discussed in §E.3).

In the first TDD period, the UE receives a grant (⑤ in Fig. 17). Subsequent UL slots in the same and following periods are also granted (⑥–⑧), since the gNB can allocate multiple outstanding grants until the buffer is emptied. A more

relaxed case is shown in Fig. 17, where new grants (⑨–⑪) arrive in each TDD period after the first. The number of granted UL slots per TDD period (assuming full allocation to the UE) is:

$$N_{UL,slots} = \min\left(\left\lceil \frac{P_{rem}}{Bi_{UL}} \right\rceil, T - d\right) \quad (38)$$

where P_{rem} is the remaining buffer, updated as data is transmitted. Thus,

$$w'_6 = N_{UL,slots} \cdot S \quad (39)$$

Finally, to compute total latency, we iterate over TDD periods, updating P_{rem} until the packet is fully transmitted. This procedure is summarized in Pseudocode 2.

E.2 UL latency when radio delay > TDD period

A special case arises when the grant (w_3 or w'_3) arrives later than the next SR opportunity, as shown in Fig. 18. Here we assume only the first UL slot per TDD period is available for SR, and a larger radio latency (①) causes the grant to be received after the next SR slot. For clarity, two RH timelines are drawn in the figure, though they represent the same RH.

In this case, since the UE has not yet received the grant for its first SR (②), it will retransmit SRs at each new opportunity (③) until the grant (④) arrives. This does not affect small packets (cf. §4.1), as the initial grant is sufficient. For large packets, however, the UE may receive multiple initial grants (④, ⑤), sending small chunks (⑥, ⑦) before larger grants (⑧–⑪) arrive. After the first major transmission (⑫), the remaining packet is transmitted in subsequent TDD periods (⑬–⑮), as in §E.1.

The procedure to compute the latency with repeated SRs is given in Pseudocode 3 and Pseudocode 4. The first algorithm identifies all SR opportunities before the first large

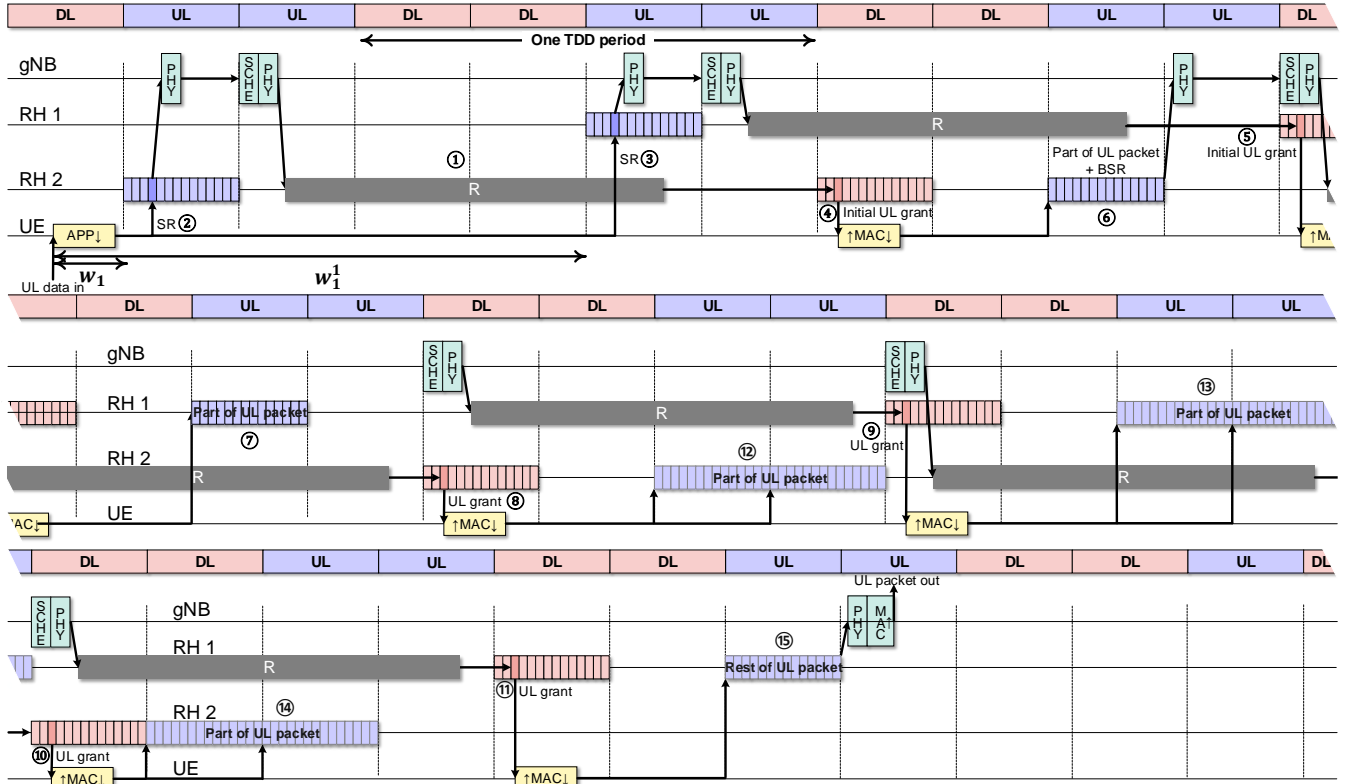


Figure 18: Journey of a packet for larger packets for the special case of extended grant latency.

grant, producing the set W_1 (e.g., w_1, w_1^1 in Fig. 18). The second algorithm then iterates over W_1 , tracking the buffer and absolute times until the packet is fully transmitted. Finally, the procedure is: run Pseudocode 3 to check whether there are single or multiple SRs, and then apply Pseudocode 2 or Pseudocode 4, respectively.

E.3 UL latency for a packet train in TDD

In this section, we extend our analysis to multiple packets that arrive dynamically at the UE and are transmitted over the same TDD uplink channel. Previously, we assumed that when a new packet arrived at the UE’s RLC buffer, no other packet was present. Under this assumption, each packet could be analyzed independently, allowing concurrent evaluation to accelerate computation. To capture interactions in the multi-packet case, we model the per-byte evolution in the RLC buffer as a finite-state machine with the following states.

- S_0 (Arrived): The byte has just entered the buffer and has not yet been requested, reported, or granted.
- S_1 (Requested): The byte was present when the UE sent the scheduling request (SR).

- S_2 (Reported): The byte was present when the UE computed and sent the buffer status report (BSR).
- S_3 (Granted): The byte is read for transmission based on resources granted to the UE.

We derive the finite-state machine shown in Fig. 19, which characterizes the possible byte states in the UE’s RLC buffer. The hatched states indicate that those bytes may or may not be present. We implement this machine in Python and use it to evaluate scenarios with multiple packet arrivals, including *Zoom* traffic and *Dota 2* multiplayer gaming traffic, as reported in Fig. 4.

E.4 UL Grant-Free Access

In uplink grant-free access, no grant message is sent by the gNB; instead, the UE uses predefined resources and slots. Thus, $w_3, w_4,$ and w_5 are not applicable, and the first transmission latency is:

$$\text{First Transmission UL Latency in Grant-Free} = w_1 + w_6 + w_7 \quad (41)$$

Here, w_1 is the wait for the next pre-configured slot, modeled as in Eq. (2)-Eq. (7) using the offset and periodicity of pre-configured grants. If one slot is insufficient, the UE repeats the process until all data is sent, as shown in Pseudocode 5. The capacity of each pre-configured slot is denoted by $B_{i_{UL}}$.

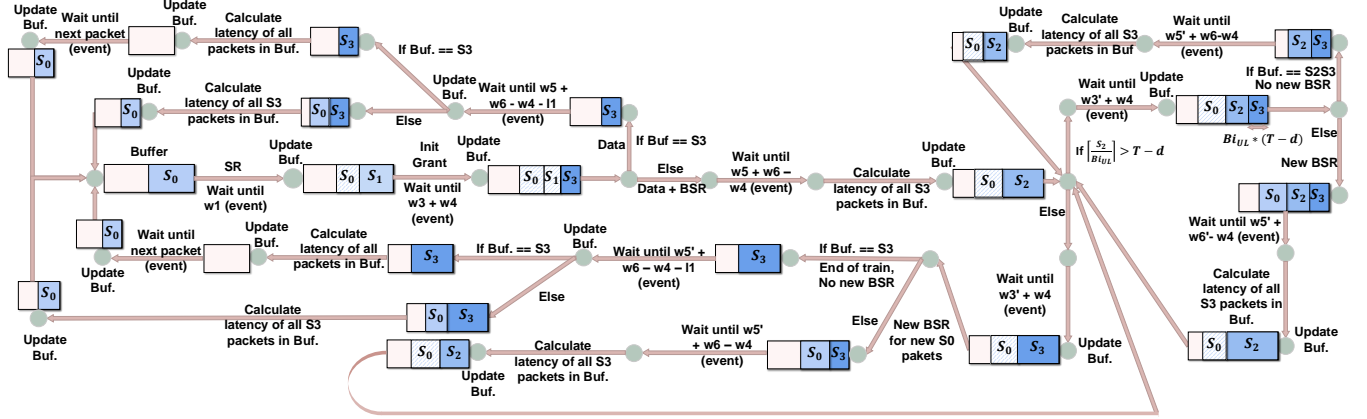


Figure 19: Finite-state machine of RLC-buffer byte states for a user.

Pseudocode 2 Total Latency of UL for Size 2 Packets with a Single Scheduling Request in TDD

```

1: Initialize  $o_1 \leftarrow t_{arrival}$ 
2: Calculate  $w_1, w_2, w_3, w_4, w_5, w_6$  (Eq. (2) to Eq. (28))
3: Initialize  $Time \leftarrow o_1 + w_1 + w_3 + w_5 + w_6$ 
4: Initialize  $P_{rem} \leftarrow P - gI$ 
5: Calculate  $w'_3$  (Eq. (29) to Eq. (32)) by substituting  $Time \rightarrow o_1 + w_1 + w_3 + w_5 + w_6$ 
6: Update  $Time \leftarrow Time + w'_3$ 
7: Calculate  $w'_5$  (Eq. (33) to Eq. (36)) by substituting  $Time \rightarrow o_1 + w_1 + w_3 + w_5 + w_6 + w'_3$ 
8: Update  $Time \leftarrow Time + w'_5$ 
9: Calculate  $B_{UL}$  (Eq. (37))
10: Calculate  $N_{UL,slots}$  (Eq. (38)) using  $P_{rem}$ 
11: Calculate  $w'_6$  (Eq. (39)) by using  $N_{UL,slots}$ 
12: Update  $P_{rem} \leftarrow P_{rem} - N_{UL,slots} \cdot B_{UL}$ 
13: Update  $Time \leftarrow Time + w'_6$ 
14: if  $P_{rem} \leq 0$  then
15:   Calculate  $w_7$  (Eq. (28))
16:   return  $Total\_Latency \leftarrow Time + w_7 - o_1$ 
17: end if
18: while True do
19:   Update  $Time \leftarrow Time + d \cdot S$ 
20:   Calculate  $N_{UL,slots}$  (Eq. (38)) using  $P_{rem}$ 
21:   Calculate  $w'_6$  (Eq. (39)) by using  $N_{UL,slots}$ 
22:   Update  $P_{rem} \leftarrow P_{rem} - N_{UL,slots} \cdot B_{UL}$ 
23:   Update  $Time \leftarrow Time + w'_6$ 
24:   if  $P_{rem} \leq 0$  then
25:     Calculate  $w_7$  (Eq. (28))
26:     return  $Total\_Latency \leftarrow Time + w_7 - o_1$ 
27:   end if
28: end while

```

E.5 DL latency in TDD

So far, we have modeled uplink latency. We now extend the model to the downlink (DL) in a TDD configuration. Since

Pseudocode 3 Calculation of the Start of Repeated Scheduling Requests for TDD UL

```

1:  $w_1^0 \leftarrow w_1$ 
2: Initialize  $j = 1$ 
3: while True do
4:   Compute  $SR_{ready}^j$  similar to Eq. (5):
      
$$SR_{ready}^j = \left\lfloor \frac{o_1 + \sum_{i=0}^{j-1} w_1^i}{S} \right\rfloor - SR_0 \quad (40)$$

5:   Compute  $q^j$  based on Eq. (6) by substituting  $q^j \rightarrow q$  and  $SR_{ready}^j \rightarrow SR_{ready}$ 
6:   Compute  $r^j$  based on Eq. (6) by substituting  $r^j \rightarrow r$  and  $SR_{ready}^j \rightarrow SR_{ready}$ 
7:   Compute  $w_1^j$  based on Eq. (7) by substituting  $w_1^j \rightarrow w_1$  and  $r^j \rightarrow r$ 
8:   if  $w_1^j > w_3$  then
9:      $SR_{num} \leftarrow j$ 
10:     $W_1 \leftarrow \{w_1^0, w_1^1, \dots, w_1^{SR_{num}-1}\}$ 
11:    return  $W_1, SR_{num}$ 
12:   else
13:      $j \leftarrow j + 1$ 
14:   end if
15: end while

```

the gNB knows all DL demands, no scheduling request is needed, making DL latency lower and the model simpler. As in §4.1, we decompose the latency into components shown in Fig. 2.

Modeling of u_1 : Time from packet arrival at the gNB to the start of scheduling. With p_5 as gNB processing time,

$$u_1 = \left(\left\lceil \frac{o_1 + p_5}{S} \right\rceil \cdot S \right) - o_1 \quad (42)$$

Modeling of u_2 : Time from scheduling start to the start of DL transmission. Ensuring it falls in a DL slot, we write:

$$re_1 \equiv_T \frac{o_1 + u_1}{S} + a_1 + 1 \quad (43)$$

Pseudocode 4 Total Latency of UL for Size 2 Packets with Multiple Scheduling Requests in TDD

```

1: Initialize  $P_{rem} \leftarrow P$ ,  $o_1 \leftarrow t_{arrival}$ 
2: Initialize  $Time$ : An array of size  $SR_{num}$  with all elements set to  $o_1$ 
3: for  $w_1^i \in W_1$  do
4:   Calculate  $w_2, w_3, w_4, w_5, w_6$  (Eq. (8) to Eq. (28)) by substituting  $w_1^i \rightarrow w_1$ 
5:   Update  $Time[i] \leftarrow Time[i] + w_1^i + w_3 + w_5 + w_6$ 
6:   Update  $P_{rem} \leftarrow P_{rem} - g_I$ 
7:   if  $P_{rem} \leq 0$  then
8:     Calculate  $w_7$  (Eq. (28))
9:      $Total\_Latency \leftarrow Time[i] + w_7 - o_1$ 
10:    return  $Total\_Latency$ 
11:  end if
12: end for
13: Calculate  $w_3'$  (Eq. (29) to Eq. (32)) by substituting  $Time[0] \rightarrow o_1 + w_1 + w_3 + w_5 + w_6$ 
14: Update  $Time[0] \leftarrow Time[0] + w_3'$ 
15: Calculate  $w_5'$  (Eq. (33) to Eq. (36)) by substituting  $Time[0] \rightarrow o_1 + w_1 + w_3 + w_5 + w_6 + w_3'$ 
16: Update  $Time[0] \leftarrow Time[0] + w_5'$ 
17: Calculate  $B_{UL}$  (Eq. (37))
18: Calculate  $N_{UL,slots}$  (Eq. (38)) by substituting  $P_{rem} \rightarrow (P_{rem} - g_I)$ 
19: Update  $P_{rem} \leftarrow P_{rem} - N_{UL,slots} \cdot B_{UL}$ 
20: Update  $Time[0] \leftarrow Time[0] + w_6'$ 
21: if  $P_{rem} \leq 0$  then
22:   Calculate  $w_7$  (Eq. (28))
23:    $Total\_Latency \leftarrow Time[0] + w_7 - o_1$ 
24:   return  $Total\_Latency$ 
25: end if
26: while True do
27:   Update  $Time[0] \leftarrow Time[0] + d \cdot S$ 
28:   Calculate  $N_{UL,slots}$  (Eq. (38)) by substituting  $P_{rem} \rightarrow (P_{rem} - g_I)$ 
29:   Calculate  $w_6'$  (Eq. (39)) by using  $N_{UL,slots}$ 
30:   Update  $P_{rem} \leftarrow P_{rem} - N_{UL,slots} \cdot B_{UL}$ 
31:   Update  $Time[0] \leftarrow Time[0] + w_6'$ 
32:   if  $P_{rem} \leq 0$  then
33:     Calculate  $w_7$  (Eq. (28))
34:     return  $Total\_Latency \leftarrow Time[0] + w_7 - o_1$ 
35:   end if
36: end while

```

$$u_2 = \begin{cases} (a_1 + 1)S, & re_1 \leq d; \\ (a_1 + 1 + (T - re_1))S, & \text{otherwise.} \end{cases} \quad (44)$$

Pseudocode 5 UL Total Latency for Grant-Free Access in TDD

```

1: Initialize  $Time \leftarrow o_1 + w_1 + w_6$ 
2: Initialize  $P_{rem} \leftarrow P - Bi_{UL}$ 
3: if  $P_{rem} \leq 0$  then
4:   return  $Total\_Latency \leftarrow Time + w_7 - o_1$ 
5: end if
6: while True do
7:   Calculate  $w_1$  based on the next pre-defined slot
8:   Calculate  $w_6$ 
9:   Update  $Time \leftarrow Time + w_1 + w_6$ 
10:  Calculate  $Bi_{UL}$  based on pre-defined resources for the slot
11:  Update  $P_{rem} \leftarrow P_{rem} - Bi_{UL}$ 
12:  if  $P_{rem} \leq 0$  then
13:    return  $Total\_Latency \leftarrow Time + w_7 - o_1$ 
14:  end if
15: end while

```

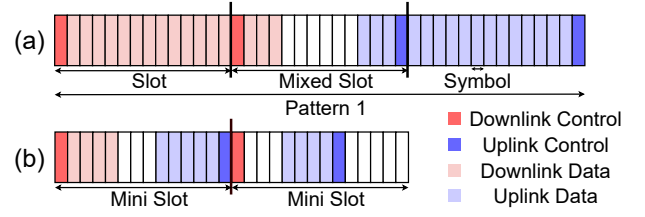


Figure 20: Comparison of (a) *Common Configuration* and (b) *Mini Slot* in TDD

Modeling of u_3 : DL transmission time, proportional to the number of DL slots:

$$u_3 = N_{DL,slots} \cdot S \quad (45)$$

Modeling of u_4 : UE processing time after receiving DL data:

$$u_4 = l_3 \quad (46)$$

Modeling the rest of the transmissions: If one TDD period is insufficient, the process mirrors UL Size-2 packets (§E.1). The DL slot capacity and number of required slots are:

$$Bi_{DL} = N_{RB}[B, T] \cdot 12 \cdot Q_m[I_{MCS}] \cdot R[I_{MCS}] \cdot (14 - DC_{no}) \quad (47)$$

$$N_{DL,slots} = \min\left(\left\lceil \frac{P_{rem}}{Bi_{DL}} \right\rceil, d\right) \quad (48)$$

As in §E.1, an iterative procedure updates P_{rem} across TDD periods until the packet is fully sent, as shown in Pseudocode 6.

E.6 UL and DL Latency in Mini-Slot Configuration

The 5G *Mini-Slot* configuration enables finer scheduling: each slot is split into DL symbols, guard symbols, and UL

Pseudocode 6 DL Total Latency in TDD

```

1: Initialize  $Time \leftarrow o_1 + u_1 + u_2$ 
2: Initialize  $P_{rem} \leftarrow P$ 
3: Calculate  $B_{DL}$  (Eq. (47))
4: Calculate  $N_{DL,slots}$  (Eq. (48)) using  $P_{rem}$ 
5: Calculate  $u_3$  (Eq. (45)) using  $N_{DL,slots}$ 
6: Update  $P_{rem} \leftarrow P_{rem} - N_{DL,slots} \cdot B_{DL}$ 
7: Update  $Time \leftarrow Time + u_3$ 
8: if  $P_{rem} \leq 0$  then
9:   Calculate  $u_4$  (Eq. (46))
10:  return  $Total\_Latency \leftarrow Time + u_4 - o_1$ 
11: end if
12: while True do
13:   Update  $Time \leftarrow Time + (T - d) \cdot S$ 
14:   Calculate  $N_{DL,slots}$  (Eq. (48)) using  $P_{rem}$ 
15:   Calculate  $u_3$  (Eq. (45)) using  $N_{DL,slots}$ 
16:   Update  $P_{rem} \leftarrow P_{rem} - N_{DL,slots} \cdot B_{DL}$ 
17:   Update  $Time \leftarrow Time + u_3$ 
18:   if  $P_{rem} \leq 0$  then
19:     Calculate  $u_4$  (Eq. (46))
20:     return  $Total\_Latency \leftarrow Time + u_4 - o_1$ 
21:   end if
22: end while

```

symbols (Fig. 20). Unlike the *Common Configuration*, every slot can carry both DL and UL traffic, which simplifies latency modeling. The gNB signals the slot format to UEs via downlink control information (DCI) on the PDCCH.

Uplink Latency: Every slot is an UL opportunity, so modeling follows §4.1 with simpler constraints:

Modeling of w_1 : Any slot can host SR, so $A = \{1, \dots, T\}$. w_1 can be calculated from Eq. (7).

Modeling of w_2 : For w_2 , the difference from the *Common Configuration* is that in *Mini Slot*, UC_{st} must start no earlier than the first UL symbol Sy_{fUL} . Thus, w_2 is as follows with this added constraint.

$$w_2 = \frac{UC_{st} + UC_{no}}{14} S, \quad UC_{st} + UC_{no} \leq 14, \quad UC_{st} \geq Sy_{fUL} \quad (49)$$

Modeling of w_3 : Since every slot is also DL, w_3 is simpler than in the *Common Configuration*: no DL-slot check is needed.

$$w_3 = (\lceil \frac{w_2 + p_1}{S} \rceil + a_1 + 1) S \quad (50)$$

Modeling of w_4 : w_4 is computed from Eq. (14), with the added requirement that the PDCCH length not exceed the DL symbols in the slot, i.e.,

$$DC_{no} \leq Sy_{IDL}. \quad (51)$$

Modeling of w_5 : With every slot valid for DL, no DL-slot check is needed. Thus, using Eq. (15):

$$k_2 = k_{2min}, \quad w_5 = k_2 S \quad (52)$$

Modeling of w_6 : UL transmission may end before the slot boundary, so w_6 can be smaller than S :

$$w_6 = \frac{Sy_{UL}}{14} S \quad (53)$$

Modeling of w_7 : w_7 is calculated based on Eq. (28).

Modeling of w'_3 : Since every slot is DL:

$$w'_3 = (\lceil \frac{p_1}{S} \rceil + a_1 + 1) S \quad (54)$$

Modeling of w'_5 : Since every slot is UL, from Eq. (33):

$$k_2 = k'_{2min}, \quad w'_5 = k_2 S \quad (55)$$

Modeling the rest of the transmissions: As in §E.2, after w'_5 every slot can be used for UL. Since each slot has both DL and UL, the same reasoning applies slot by slot. With Sy_{fUL} and Sy_{lUL} as the first and last UL symbols, the per-slot payload is:

$$Bi_{UL} = N_{RB}[B, T] \cdot 12 \cdot Q_m[LMCS] \cdot R[LMCS] \cdot (Sy_{lUL} - Sy_{fUL} + 1 - UC_{no}) \quad (56)$$

The remaining transmissions are then obtained iteratively as in Pseudocode 7.

Pseudocode 7 UL Total Latency with *Mini Slot* Configuration in TDD and UL Total Latency in FDD

```

1: Initialize  $P_{rem} \leftarrow P - g_I$ 
2: if  $P_{rem} \leq 0$  then
3:   Calculate  $w_1, w_2, w_3, w_4, w_5, w_7$ 
4:   Calculate  $w_6$  according to the selected duplexing mode (Mini-slot vs. FDD)
5:   return  $Total\_Latency \leftarrow w_1 + w_3 + w_5 + w_6 + w_7$ 
6: end if
7: Calculate  $w_3, w_5, w'_3,$  and  $w'_5$ 
8: Initialize  $Time \leftarrow o_1 + w_1 + w_3 + w_5 + S$ 
9: Update  $Time \leftarrow Time + w'_3 + w'_5$ 
10: while True do
11:   Calculate  $Bi_{UL}$  based on Eq. (56) in the case of Mini Slot and Eq. (37) in the case of FDD
12:   Update  $P_{rem} \leftarrow P_{rem} - Bi_{UL}$ 
13:   if  $P_{rem} \leq 0$  then
14:     Calculate  $w_6$  according to the selected duplexing mode (Mini-slot vs. FDD)
15:     Calculate  $w_7$ 
16:     return  $Total\_Latency \leftarrow Time + w_6 + w_7 - o_1$ 
17:   end if
18:   Update  $Time \leftarrow Time + S$ 
19: end while

```

Downlink Latency: DL latency in the *Mini Slot* configuration follows the same approach as §E.5, with simplified constraints.

Modeling of u_1 : u_1 can be calculated using Eq. (42).

Modeling of u_2 : Every slot includes DL, so:

$$u_2 = (a_1 + 1)S \quad (57)$$

Modeling of u_3 : Transmission time depends on the number of DL symbols:

$$u_3 = \frac{Sy_{DL}}{14}S \quad (58)$$

Modeling of u_4 : u_4 can be calculated using Eq. (46).

Modeling the rest of the transmissions: Since each slot starts with a DL symbol, defining the number of DL symbols in the slot as Sy_{fDL} , then the value of Bi_{DL} can be calculated as follows:

$$Bi_{DL} = N_{RB}[B, T] \cdot 12 \cdot Q_m[I_{MCS}] \cdot R[I_{MCS}] \cdot (Sy_{fDL} - DC_{no}) \quad (59)$$

The remaining latency is then computed iteratively as in Pseudocode 8.

Pseudocode 8 DL Total Latency with *Mini Slot* Configuration in TDD and DL Total Latency in FDD

- 1: Calculate u_1 and u_2 based on Eq. (42) and Eq. (57)
 - 2: Calculate Bi_{DL} based on Eq. (59)
 - 3: Initialize $P_{rem} \leftarrow P - Bi_{DL}$
 - 4: **if** $P_{rem} \leq 0$ **then**
 - 5: Calculate u_3 according to the selected duplexing mode (Mini-slot vs. FDD)
 - 6: Calculate u_4 based on Eq. (46)
 - 7: **return** $Total_Latency \leftarrow u_1 + u_2 + u_3 + u_4$
 - 8: **end if**
 - 9: Initialize $Time \leftarrow u_1 + u_2 + S$
 - 10: **while** True **do**
 - 11: Calculate Bi_{DL} based on Eq. (59) in the case of Mini Slot and Eq. (47) in the case of FDD
 - 12: Update $P_{rem} \leftarrow P_{rem} - Bi_{DL}$
 - 13: **if** $P_{rem} \leq 0$ **then**
 - 14: Calculate u_3 according to the selected duplexing mode (Mini-slot vs. FDD)
 - 15: Calculate u_4 based on Eq. (46)
 - 16: **return** $Total_Latency \leftarrow Time + u_3 + u_4$
 - 17: **end if**
 - 18: Update $Time \leftarrow Time + S$
 - 19: **end while**
-

E.7 UL and DL latency in FDD

In FDD,⁷ uplink and downlink use separate frequency bands, so each slot is simultaneously a full DL and a full UL slot.

Uplink Latency: FDD modeling mirrors the *Mini Slot* case: - $w_1, w_3, w_5, w'_3,$ and w'_5 from Eq. (7) (with $A = \{1, \dots, T\}$),

⁷FDD is only supported in sub-2.6 GHz bands [4], typically used by public operators. Private 5G deployments are allocated bands that only support TDD, so for URLLC applications such as industrial automation [13] and hospitals [42], TDD is the practical option.

Eq. (50), Eq. (52), Eq. (54), and Eq. (55). - Since all symbols are UL: - $w_2, w_4, w_7,$ and Bi_{UL} from Eq. (8), Eq. (14), Eq. (28), and Eq. (37). - $w_6 = S$. The total UL latency is then computed as in Pseudocode 7.

Downlink Latency: Again similar to *Mini Slot*: - $u_1, u_2,$ and u_4 from Eq. (42), Eq. (57), and Eq. (46). - Since all symbols are DL: - Bi_{DL} from Eq. (47). - $u_3 = S$. The total DL latency is then computed as in Pseudocode 8.

E.8 UL latency under multi-UE contention

We extend the single-UE multi-packet model from §E.3 to the case of multiple UEs transmitting over the same channel. Contention occurs whenever the total requested resources exceed the available resources within a single slot. In this case, packet latency depends on the gNB scheduling policy. We model contention under a round-robin scheduler. In each slot, UEs are ordered by ID and granted resources sequentially until the slot resources are exhausted. The ordering is shifted by one UE in every slot, ensuring fairness over time. While we focus on round-robin scheduling in this work, one can extend the model to more scheduling policies. However, we leave such extensions to future work which may incorporate other schedulers by modifying the resource allocation rule among contending UEs.

Contention modeling procedure. First, we run the single-UE model for each UE independently, assuming no contention. This yields, for every packet, its transmission start time and latency baseline. Next, we identify overlaps across UE transmissions and partition the timeline into segments. Within a segment where exactly N UEs contend, each UE receives on average a fraction $\frac{1}{N}$ of its requested resources. Therefore, a segment of nominal duration L is stretched under contention to $N \cdot L$.

Packet latency is then recomputed by summing over all stretched segments.

Additional TDD delay. In TDD configuration, there is another contention effect due to limited uplink slots. For example, consider $N = 4$ contending UEs using a TDD configuration with period $T = 10$ slots, of which only $U = 3$ slots are uplink. Since only three UEs can be scheduled per period, one UE would not be scheduled in each period. Thus, every UE experiences an additional delay of one full TDD period every four periods, increasing packet latency beyond the resource-sharing effect. Let the TDD period be T slots, containing U uplink slots.

In every N TDD periods, there are exactly $N - U$ periods in which a UE is not scheduled in uplink (assuming full utilization by others). If a packet requires total transmission time t slots, the additional delay due to missed UL turns is

$$\left\lfloor \frac{t}{NT} \right\rfloor (N - U)T \quad (60)$$

Final latency. The final packet latency under contention is the sum of (i) the baseline latency without contention, (ii) the segment expansion due to resource sharing, and (iii) the additional TDD delay:

$$\text{Latency} = \text{Latency}_{\text{no cont.}} + \text{Delay}_{\text{resource}} + \left\lfloor \frac{t}{NT} \right\rfloor (N - U)T \quad (61)$$